CHAPTER 9
Molecular Surfaces

9.1 Introduction

In the case of a simple single crystal such as sodium chloride (Chapter 1), the surface can be pictured as being a plane of uniformly spaced atoms. This is a very simplistic view of a single crystal surface and in reality it will be decorated with defects. The morphology of a solid is dictated by a series of dynamic and thermodynamic factors and can be influenced by the specific interactions that are associated with the surface. Gibbs recognized that the free energy of the interface can be significantly different from that of the bulk. The energy of the interface reflects the imbalance of forces acting on the molecules located at the boundary. Technologically the nature of the surface can have profound effects on physical properties such as wear, adhesion and friction and subjective properties such as gloss and appearance. In order to understand the properties of the interface it is necessary to consider the balance of forces that exist in the region of the interface. There are three types of interface that need to be considered: solid–liquid, solid–air and solid–solid. The latter, solid–solid, was introduced when considering copolymer blends in Chapter 8. The design of the interface between a polymer and another material can be critical to the use of that polymer in a specific application, in particular in adhesion science.

9.2 Gibbs Approach to Surface Energy

In the case of the polymer–air interface, the ability to stick to the surface, resist wear or have a certain aesthetic characteristic can be dependent on the way the polymer molecules are organized at the interface. A number of physical phenomena are related to our understanding of the properties of an interface: spreading of oil on a surface, adhesion of two bodies in contact (e.g. chewing gum sticking to a pavement), interaction of fluids with biological materials (e.g. blood in arteries), *etc*.

At a molecular scale an interface is an imbalanced system of interactions and will have an associated imbalance of chemical potential and free energy. The molecules at the air–solid surface are attracted by the molecules in the bulk and

are unable to escape. As discussed in Chapter 1, a simple molecule in the 'bulk' will be surrounded by a number of molecules that reflect the crystal packing geometry. In a typical face-centred cubic (fcc) arrangement we might have 14 nearest neighbouring molecules. To create the surface, half of the unit cell is removed so that now the number of interacting nearest neighbours is reduced to 11. The balance of the forces on the molecule will be to attract the molecule into the bulk. Molecules will prefer to be 'in the bulk' since they would be thermodynamically more stable if they are completely surrounded by other molecules.

Similar imbalances of forces will exist at the liquid–solid and the solid–solid interfaces. In the case of the liquid–liquid or liquid–solid interfaces when the energies of the two phases approach one another then mixing can occur. If the two phases have essentially the same energy then mutual diffusion will occur and a homogeneous mixture can be created. Liquid will mix with other liquid if their energies a similar and the surface tension is low.

9.2.1 Contact Between a Liquid and a Surface

Many of the important features of the interface can be understood by considering the problem of a liquid drop in contact with a surface (Figure 9.1). Gibbs defined a parameter, the *surface tension*, designated as γ, to represent the imbalance of forces at the interface.

Surface tension is defined in terms of the energy change that is required to produce a new surface. The work is equal to $F\mathrm{d}x$, where $\mathrm{d}x$ is the movement in the direction perpendicular to the surface and F is the force created by the molecules in the bulk. Therefore $F\mathrm{d}x = \gamma\mathrm{d}A$, where $\mathrm{d}A$ is the change in area of the surface and γ is the surface tension which has dimensions of force per unit distance, mN m^{-1}. Typical values of the surface tension of some common liquids are summarized in Table 9.1.

9.2.2 Derivation of Young's Equation and Definition of Contact Angle

With regard to the schematic in Figure 9.1, consider the following interfaces: the liquid and solid, the liquid and gas, and the solid and gas. At the point a the three phases connect and the forces must balance if the system is at equilibrium. The forces can be resolved into components parallel to the substrate and
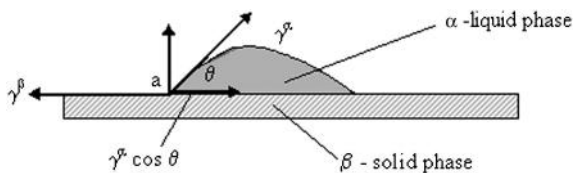

Figure 9.1   Schematic of a liquid droplet in contact with a solid surface.

Table 9.1 Values of surface tension of some common liquids and an indication of the dominant interactions.

Liquid (type of molecule)	γ (mN m^{-1})	Force involved in surface tension
Mercury (Hg)	476	Metallic
Water (H$_2$O)	72.75	Hydrogen bonds
Octane (C$_8$H$_{18}$)	21.69	van der Waals
Benzene (C$_6$H$_6$)	28.88	van der Waals+π–π induced dipole interactions
Carbon tetrachloride (CCl$_4$)	26.77	van der Waals+collisional dipole interactions

perpendicular to the substrate. The labels are respectively for the surface tension of the liquid–air interface, γ^α; solid–air interface, γ^β; and solid–liquid interface, $\gamma^{\alpha\beta}$. When the droplet is at equilibrium, *Young's equation* applies:

$$\gamma^\beta = \gamma^{\alpha.\beta} + \gamma^\alpha \cos\theta \qquad (9.1)$$

The measurement of the force $\gamma^{\alpha\beta}$ is not practical and hence an alternative approach is usually adopted. The work of adhesion that involves removal of the liquid from the solid can be shown to be equal to the work required to create a new surface from a column of a fluid:

$$W = \gamma^\alpha + \gamma^\beta - \gamma^{\alpha\beta} \qquad (9.2)$$

This work of adhesion can be combined with the Young equation:

$$W = \gamma^\alpha + \gamma^\beta - \gamma^{\alpha\beta} + \gamma^\alpha \cos\theta - \gamma^{\alpha\beta} \qquad (9.3)$$

where θ is the angle between the liquid surface and the substrate. Thence

$$W = \gamma^\alpha - \gamma^\alpha \cos\theta \qquad (9.4)$$

which is the work associated with the sticking of the liquid to the surface. The parameter θ has values that lie between 0° and 180°, and defines whether or not a liquid will wet a substrate:

(a) spreading film
$\theta = 0°$, cos $\theta = 1$

(b) wetting droplet
$\theta = 90°$, cos $\theta = 0$

(c) non-wetting droplet
$\theta = 180°$, cos $\theta = -1$

$W^{\alpha\beta} = 2\gamma^\alpha$ (wetting)
$\theta < 90°$

$W^{\alpha\beta} = \gamma^\alpha$
$\theta = 90°$

$W^{\alpha\beta} = 0$ (non-wetting)
$\theta > 90°$

The work of cohesion, the material with itself, is equal to $2\gamma^\alpha$ and has a contact angle of 0°. In general for a simple fluid the work of adhesion and cohesion are equal and for $\theta < 90°$, the liquid is *wetting* the solid and when $\theta > 90°$ the liquid

is *not wetting* the solid. In the simplest example, silicone oil that will lower the surface energy could be present as a contaminant.

This situation can be depicted as shown below; the differently shaded bars illustrate the variation in the surface energy:
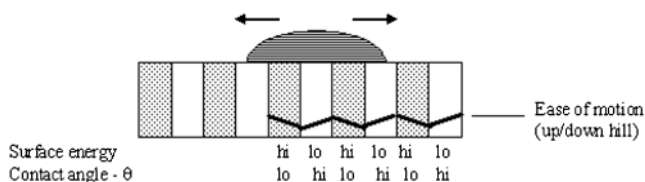
As the size of the droplet increases, the contact angle will vary reflecting the nature of the surface energy immediately at the point of contact between the three phases. If the droplet size is now reduced 'hysteresis' effects can be observed. The liquid having wet the surface may detach leaving a molecular thin layer on the substrate. The effective surface energy is now that of the detaching liquid from the molecular absorbed layer and not that of the solid. The contact angle for the droplet reducing the advancing contact angle θ_a is greater than the retarding contact angle θ_r. The important factor in determining the nature of the process is the relative magnitude of the attraction of the liquid molecules for each other compared to the intermolecular forces across the liquid–solid interface at any given point on the solid surface:
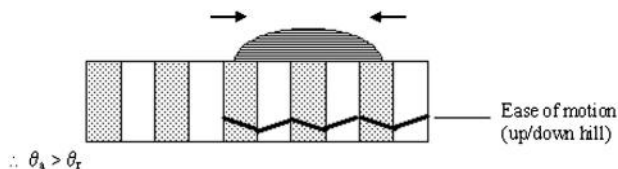
The drop will readily leave the low-energy patch but will not want to move off the high-energy patch; hence θ_r is slightly smaller than θ_a.

Measurements of hexamethylethane, C_8H_{18}, indicate a contact angle of $\theta = 115°$, whereas a C_{16} cycloparaffin has a value of $\theta = 105°$, indicating that in the case of C_8H_{18} the surface is made up of CH_3 groups, whereas in the case of the cycloparaffin the surface is covered with CH_2 groups. The C_{16} cycloparaffin is more readily wetted by water than C_8H_{18}. This technique can be used to determine the difference in the surface tension between different organic compounds.

In the presence of a surface, the total Gibbs free energy includes the normal bulk free energy terms and an additional free energy term which is associated with the creation of the interface:

$$G = H - TS + \gamma A \tag{9.5}$$

where G is the Gibbs free energy, S is the entropy, H is the enthalpy and T is the temperature. The surface tension has the following thermodynamic definition:

$$\gamma = \left(\frac{\partial G}{\partial A}\right)_{T,P} \tag{9.6}$$

The associated thermodynamic properties are as follows for the entropy and enthalpy:

$$\Delta S = -\frac{\partial \gamma}{\partial T} \quad \text{and} \quad \Delta H = \gamma - T\frac{\partial \gamma}{\partial T} \tag{9.7}$$

This classical definition is for any interface. The interfacial energy is a consequence of the interaction between molecules and contains contributions from mutually attractive intermolecular forces due to combined effects of dispersions, dipole, induced dipole and hydrogen bonding interactions. At short distances molecular species are repulsive whereas at longer distances the molecules become attractive. A variety of different interaction potentials can be used; however, the simplest is an inverse square law, in which case the interaction energy has the form

$$W_c = \left(\frac{A}{12\pi}\right)(r_0^{-2} - r^{-2}) \tag{9.8}$$

where r is the separation distance between the entities and A is the Hamaker constant representing the cumulative strength of all types of interaction. If the separation distance is increased to infinity the macroscopic interfacial tension and the strength of the molecular interactions are related by

$$\gamma = \frac{A}{24\pi r_0^2} \tag{9.9}$$

The surface tension of a surface influences the interaction with other phases and in particular solids and liquids. A liquid in contact with a solid or another liquid will attempt to balance the energy at the interface. For a drop of liquid on an interface, the surface energy must balance and the angle it makes with the surface is defined by eqn (9.1). Spontaneous wetting of the surface will occur when $\theta = 0$. In practice, the surface tension, contact energy, is not constant but can vary across the surface as a result of either changes in composition or surface texture. For a heterogeneous surface consisting of two domains the observed contact angle θ_c is defined by

$$\cos \theta_c = f_1 \cos \theta_1 + f_2 \cos \theta_2 \tag{9.10}$$

where f_1 and f_2 are the surface fractions of components 1 and 2, and θ_1 and θ_2 are their contact angles. The differences in contact angle can reflect the presence of different atomic species or surface topography. As we will explore later,

surface contamination can have a major effect on the surface energy and contact energy.

9.3 Surface Characterization

There are a variety of different methods available for the inspection of the surface of a material.[1–13] The techniques available can be divided into groups:

(i) Classical surface assessment methods, contact angle measurements.
(ii) Visualization of the surface: optical, electron and atomic force microscopy.
(iii) Spectroscopic assessment of the surface: attenuated total reflection infrared, fluorescence and visible spectroscopy.
(iv) X-Ray and neutron diffraction analysis.
(v) Ion beam analysis: electron recoil and Rutherford backscattering.
(vi) Vacuum techniques: X-ray photoelectron spectroscopy (XPS), secondary ion mass spectroscopy (SIMS), Auger electron spectroscopy (AES).

Each of these techniques can provide information on a particular aspect of the surface and add to our understanding of the factors that influence the way molecules are arranged at a surface.

9.3.1 Classical Surface Assessment Methods, Contact Angle Measurements[4]

The simplest method of assessment of the energy of a surface involves the study of contact angles. The most obvious method is the direct measurement of the tangent between a liquid drop and a solid. A liquid drop in contact with a solid will behave according to eqn (9.4). It is possible to determine the contact angle by measuring the dimensions of a liquid drop.

For very small drops of the order of 10^{-4} ml the distorting effect of gravity is negligible and the drop takes the shape of a spherical segment. In this case, the contact angle θ can be calculated using

$$\tan\frac{\theta}{2} = \frac{h}{r} \tag{9.11}$$

or

$$\sin\theta = \frac{2hr}{h^2 + r^2} \tag{9.12}$$

where h is the drop height and r is the radius of the drop base. The drop height is usually smaller than the base radius and more difficult to measure. In such a case, the contact angle may instead be calculated for a spherical drop from the volume of the drop and its radius at its base:

$$\frac{r^3}{V_d} = \frac{3 \sin^3 \theta}{\pi(2 - 3 \cos \theta + \cos^3 \theta)} \tag{9.13}$$

where V_d is the drop volume. The contact angle can be determined to ± 2–$3°$ but depends very much on the properties of the surface: roughness uniformity, whether it absorbs the solvent, *etc*.

The energy of the surface can be obtained by observing the variation of the contact angle for liquids of different surface tension and extrapolation to a virtual contact angle of $0°$ (Figure 9.2). At a contact angle of zero the liquid spreads over the polymer surface. This value of the surface tension above which spontaneous spreading does not take place is termed the critical surface tension. The spreading coefficient, S, is defined as $S = \gamma_l(\cos \theta - 1)$ and does not imply that spreading is impossible for $\gamma_l > \gamma_c$; gravitational and other factors may cause the liquid to spread over the surface.

The absolute values of the surfaces tensions for the liquids can be determined independently allowing an unambiguous measurement of the surface tension through the contact angle. Typical values for a range of polymers are summarized in Table 9.2.

Surface roughness is an important factor in consideration of the surface tension. If we consider the surface as depicted in Figure 9.3a we can see that the roughness can effectively vary the contact angle.

If gravity is assumed not to play a role, then the observed contact angle θ_0 is given by
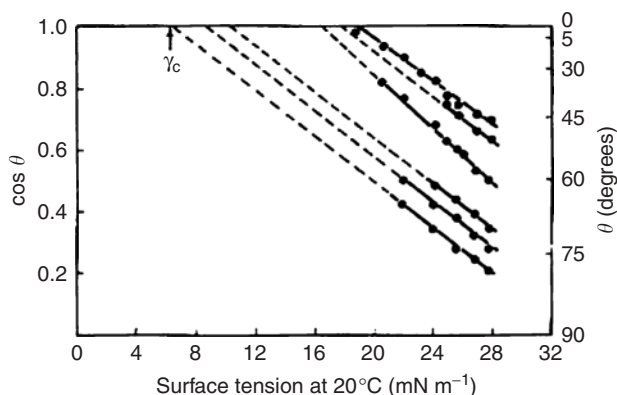
$$\theta_0 = \theta_i + \alpha \tag{9.14}$$

Figure 9.2 Contact angle on various perfluorinated low-energy surfaces of *n*-alkane liquids.[11]

Table 9.2   Critical surface tensions for some typical polymers at 20°C.

Polymer	Critical surface tension, γ_c
Polytetrafluoroethylene	18
Polytrifluoroethylene	22
Poly(vinylidene fluoride)	25
Poly(vinyl fluoride)	28
Polyethylene	31
Polytrifluorochloroethylene	31
Polystyrene	33
Poly(vinyl alcohol)	37
Poly(vinyl chloride)	39
Poly(vinylidene chloride)	40
Poly(ethylene terephthalate)	43
Poly(hexamethylene adipamide)	46

where α is the angle of inclination of the surface at the point of liquid–solid contact. The maximum and minimum observed angles are given by

$$\theta_{max} = \theta_i + \alpha_{max} \qquad (9.15)$$

and

$$\theta_{min} = \theta_i - \alpha_{max} \qquad (9.16)$$

where α_{max} is the maximum inclination of the surface. If the surface is very rough a liquid with a large equilibrium contact angle may not completely wet the surface (Figure 9.3b). The roughness can be related to the contact angle by[15]

$$\cos\theta_w = r\cos\theta \qquad (9.17)$$

where θ_w is the equilibrium contact angle on a rough surface, θ is the equilibrium contact angle observed on a smooth surface and r is the surface roughness or the average ratio of the two areas. The effect of high values of surface roughness explains the water repellent characteristics of some materials. Duck feather fibres are about 8 μm in diameter and separated at a similar distance with the effect that the effective contact angle is raised from a value for the material of 95° to a value of 150°, and so water drops just roll off. Hence the expression: 'like water off a duck's back'.

A further factor encountered in practice is the absorption of a liquid by the substrate. The adsorption will match the substrate to the fluid and the contact angle will steadily reduce and wetting will be affected. This is observed with blotting paper where the substrate absorbs the liquid with which it is in contact.

9.3.2   Visualization of the Polymer Surface

Visual or other methods of visualization of the surface can provide a significant amount of information on the nature of the surface.
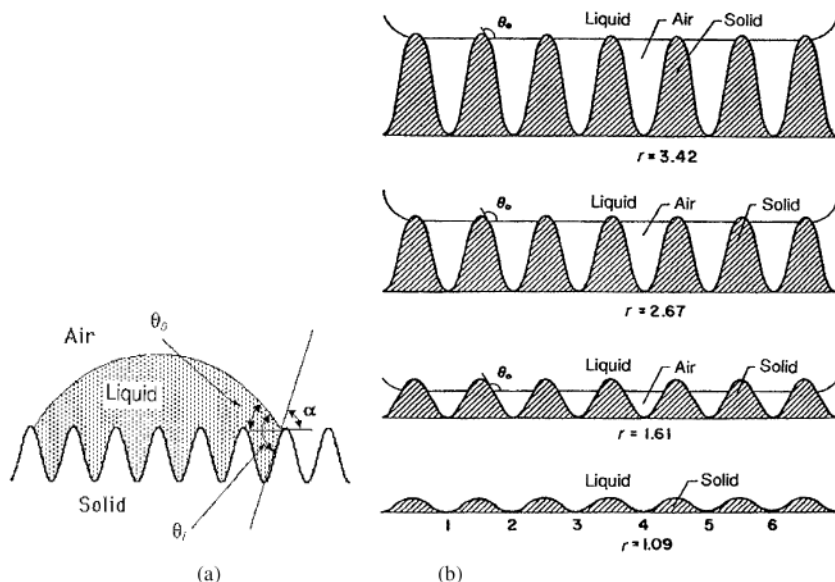
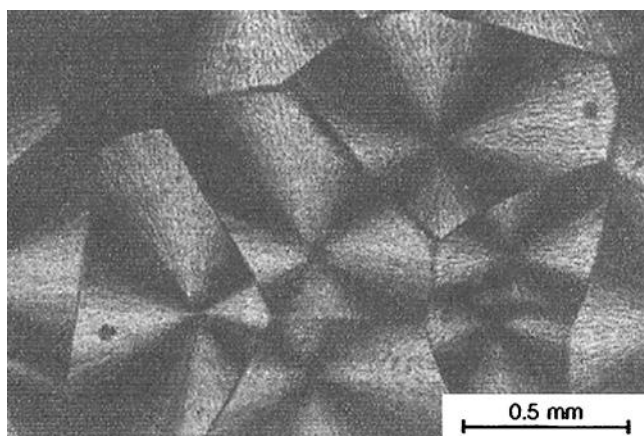**Figure 9.3**   Surface roughness and influence of roughness on wetting.[10]

Figure 9.4   Spherulite structure in poly(butane-1) after impingement.[14]

9.3.2.1   *Optical Microscopy*[14,16]

The simplest and most direct method of examination of a surface is by use of optical microscopy. Surface features of the order of 1 μm or greater are usually detectable. To achieve greater contrast, polarizing microscopy is often used.[14] In the case of liquid crystalline materials (Chapter 3), polarized microscopy, since it explores the alignment of the molecular axis, can reveal both order and alignment in materials. In the case of polymers with a polarizable group either

as part of the backbone or aligned with the chain axis, polarizing microscopy can identify regions of order (Figure 9.4).

Optical methods are useful for observation of spherulitic structures (Figure 9.4) and other forms of higher order organization but will not give information on lamellar nanoscale structures. The differences in birefringence between the different orientations adopted by the crystal lamellae as they radiate in all directions and the non-crystalline amorphous regions gives rise to a Maltese cross effect. If the lamellae twist in phase with one another then this gives rise to rings. Birefringence measurements can be made using a compensator and can provide useful information on the nature of the chain alignment in the material. In the case of materials where there is no birefringent species present, visualization of order can be achieved by absorption of a suitable birefringent molecule onto the aligned areas.

9.3.2.2   Electron Microscopy[9,15]

There are two methods of electron microscopy commonly encountered in the study of polymers: scanning electron microscopy (SEM) and scanning transmission electron microscopy (STEM). Both techniques use a focused high-energy beam of electrons to illuminate the sample which is conventionally held in a high vacuum. Recently a variant of SEM, called environmental SEM (ESEM) has been developed which allows the sample to be held at close to ambient pressures.[17] ESEM uses differential pumping to allow the electron beam to be focussed and shaped and it is only in the region of the impingement on the sample that the beam is brought to near atmospheric pressure. This technique has the attraction that it allows examination of specimens that may have their morphology changed by being exposed to high vacuum. It has allowed study of liquid droplets in contact with polymer fibres and examination of highly hydrated biological specimens.

The interaction of the electron beam with the sample can be summarized as follows:
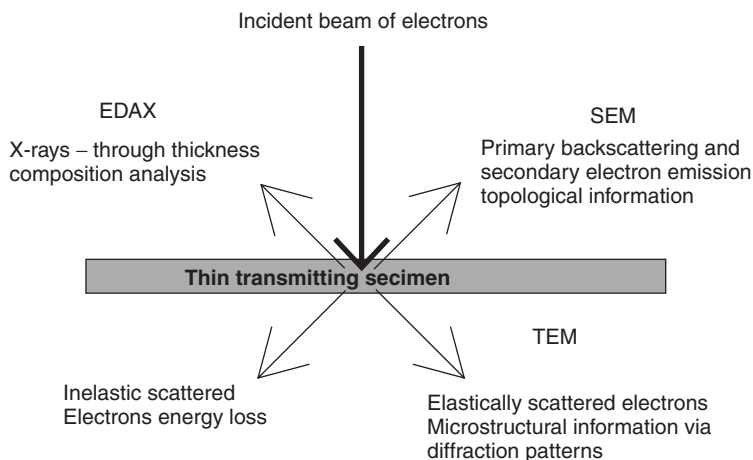
The electrons undergo a combination of inelastic and elastic scattering events. The elastically scattered electrons are collected from the back of thin samples and the diffraction patterns provide information on the crystalline structural order in the irradiated region. Using a beam of the order of 100 kV the region illuminated is ~ 0.5–70 µm diameter. Special instruments are available which provide high resolution and operate at 500 to 1000 kV. The principal difference between SEM and TEM is the thickness of the sample studied. If the sample is very thin then TEM can be used but requires the section be cut from a liquid nitrogen frozen sample using a diamond-bladed microtome.

9.3.2.3 Scanning Transmission Electron Microscopy (TEM)[9,16]

The type of instrument used for TEM is designed to give atomic resolution. The original instruments used photographic detection of the diffraction images but modern instruments use electronic imaging and allow imaging of very small features.

9.3.2.4 Scanning Electron Microscopy (SEM)[9,16]

In conventional SEM, the sample is placed in a vacuum chamber and exposed to a focused electron beam. The electron and X-ray emission are then analysed to produce a visualization of the polymer structures and atomic composition. To understand how these images are created it is necessary to consider briefly the mechanism of the interaction of the electron beam with the sample. The electron beam will typically have an energy of between 100 kV and 500 kV and is focused down to a spot that will have a cross-section of a few hundred nanometres or less depending on the resolution being sought. This high-energy beam will impinge on the sample surface and as the electrons penetrate the solid they will undergo a range of inelastic and elastic scattering events.

9.3.2.5 Inelastic Electron Scattering

Interaction with the electron cloud of the molecules can lead to a small amount of energy being transferred and the scattered electron has a slightly different energy and a change in direction compared to the incident electron. The primary electron can produce emission of secondary electrons from the atoms with which they interact. These secondary electrons will either be trapped in the solid and produce charging of the substrate or if they have sufficient energy to overcome the surface work function will escape and can be detected. The probability of scattering occurring will depend on the atomic member of the atom producing the scattering; the higher the value of Z, the greater the scattering. The secondary electrons that do not have sufficient energy to escape can be trapped in the surface and lead to surface charging. To avoid this problem, samples for SEM are often coated on a thin metal layer or have a layer of conducting graphite deposited on the surface. Provided that the surface charge is minimized then the scanning of the surface allows the atomic

distribution to be determined and images of the surface to be created. It is important to understand that the secondary electrons will come from a layer that is effectively several hundred nanometres or even micrometres deep. Although the image looks like a surface, it is in effect a composite of the events that create the secondary scattering. Some of the electrons will have sufficient energy to kick off one of the core electrons and the result will be that the subsequent relaxation of the electron structure is accompanied by the emission of an X-ray for the atom corresponding to a characteristic of a core electron transition. The X-rays are emitted from a zone that is defined in terms of the region where secondary scattering occurs and are not restricted by the constraints of the escape energy that control the secondary electron emission. As a consequence the depth probed by the X-ray emissions can be several micrometres and will be typically a cylinder of about 0.5 to 1 μm in diameter and a depth 1–2 μm. It will evident that energy dispersive X-ray analysis (EDAX) gives average data over a very significant volume and is not very specific. It is possible in favourable situations to image the surface selectively by selecting an particular X-ray line which is characteristic of that element, this approach being widely used in metals but not very useful for carbon and other low molar mass materials.

9.3.2.6 Elastic Electron Scattering

Some of the electrons are electrically scattered, *i.e.* their direction is changed without changing their energy. These scattering events occur according to Bragg's laws of diffraction and hence analysis of the scattering pattern provides information on the order of the scattering centres in the solid. Just as conventional X-ray scattering provides information on the crystalline order in solids, so electron scattering can in principle provide similar information. Unlike X-rays, the elastically scattered electrons can undergo secondary scattering and then the information on the structure is lost. Electron microscopy provides a very powerful tool for the visualization of polymer structures at the micrometre to sub-micrometre scale and has provided researchers with a wealth of data on the topography of polymer surfaces. Many apparently smooth surfaces are found to be rough when viewed at the nanometre scale (Figure 9.5).

'A picture is worth a thousand words': this is very true when it comes to understanding surface structure. A more detailed discussion of the theory and experimental methods can be found elsewhere.[16–18,9]

9.3.3 Atomic Force Microscopy[19]

An important recent addition to the methods available is atomic force microscopy (AFM).[19] This technique, as its name implies, measures the force between a fine probe that has a tip that is of sub-micrometre dimensions and the surface. There are several variations of the basic method. A simple instrument is shown diagrammatically in Figure 9.6a. The potential energy curves being sensed can be visualized as being similar to that shown in Figure 9.6b.
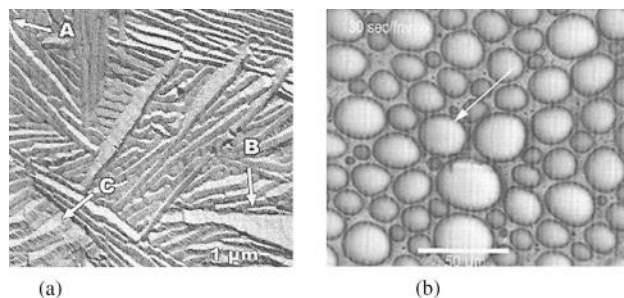
(a)   (b)

Figure 9.5   Electron micrographs of (a) an etched surface of linear polyethylene showing (A) a group of edge-on lamellae and (B) a basel surface and (C) lamellae side surfaces with striations from pulled-off molecular stems.[18] (b) ESEM of corn oil droplets in a water/oil emulsion.[17]
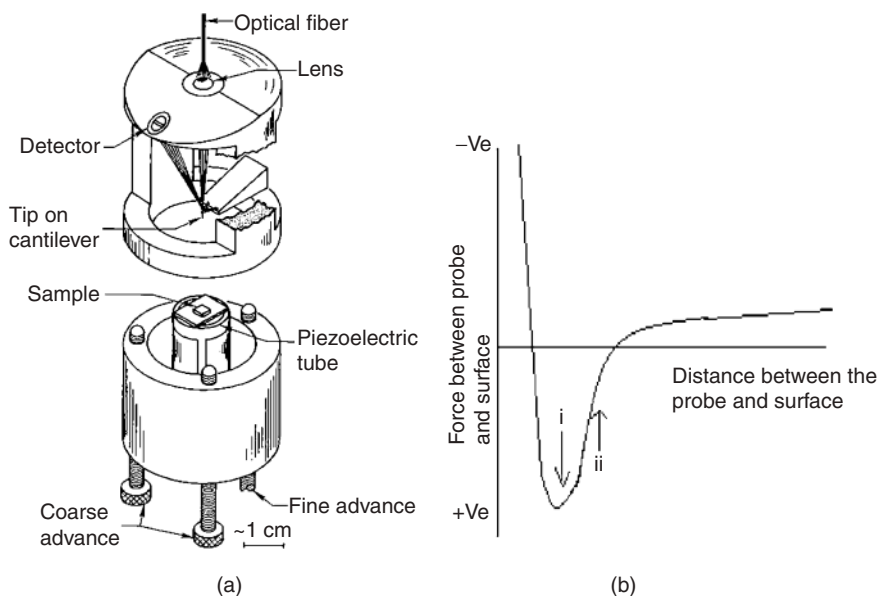

(a)   (b)

Figure 9.6   Schematic of an atomic force microscope (a) and the force profile being sensed during the scan (b).

A light beam is reflected from the scanning tip onto a quadruple detector. The detector output is able to indicate movement in the z-direction and allows the piezoelectric tube to adjust and maintain a constant distance between the tip and sample (Figure 9.5b). By mapping the variation of the force when the point is scanned across the surface, it is possible to visualize the underlying topography of the surface. The force is measured by detecting the deflection of a spring that supports the sensing element using a laser interferometer. The microfabricated cantilever has a length of only 100 μm. The optical lever ratio
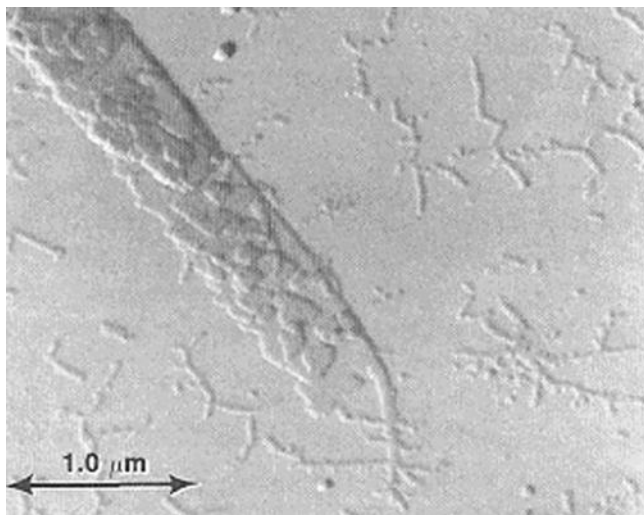
Figure 9.7   AFM image of a deposit of high molecular mass polyethylene deposited on a mica surface.[18]

used is around 800. The force with which the tip pushes against the sample is as low as 2×10^{-9} N. Various modes of scanning have been developed. The simplest is to find the minimum in the force profile in region (i) and attempt to maintain the tip at this distance. The change of force with separation, however, is not very sensitive to change in distance and hence the resolution of the scan of the surface is not very high. A higher resolution can be achieved by moving to the regions where the force profile is steeper (ii); here the movement of the tip will be more sensitive to the change in the profile. Additional sensitivity can be achieved if the tip is modulated and the so-called 'tapping' mode is adopted. Both modes of operation of the instrument allow the surface to be mapped and atomic resolution can be achieved with atomic solids. In the case of polymers the resolution that can be achieved is usually of the order of nanometres[20] (Figure 9.7). The AFM image shows isolated clusters of polymers and also an entangled collection of chains that are attempting to form an ordered structure.

A combination of optical, electron and atomic force microscopy can provide a very useful visualization of the surface of a material. It must be emphasized that each method has its strengths and weaknesses. The optical methods are unable to probe the structure below ~ 1 μm, but have the advantage of readily revealing order through the use of birefringence. Electron microscopy is capable of significantly higher resolution and can readily approach the 10 nm or better level. However, it must always be remembered that the image is the result of complex scattering processes and the height of features is often difficult to determine. AFM is capable of achieving a high resolution in the z-direction, perpendicular to the surface; however, the finite size of the tip limits the resolution of features in the x- and y-directions, although nanometre dimensions are accessible.

Whilst the above methods can provide a visualization of the surface topography, they are unable to address two questions. Firstly, they are unable to provide information on the density distribution relative to the notional surface, and secondly, they are unable to allow identification of the surface elemental, atomic, composition.

9.4 Spectroscopic Assessment of the Surface: Attenuated Total Reflection Infrared, Fluorescence and Visible Spectroscopy[16]

The infrared spectra of thin films and surfaces can be examined using attenuated total reflection (ATR) methods. Unlike conventional infrared spectroscopy the beam impinges on the surface as a consequence of being reflected from a crystal that is in contact with the surface to be examined (Figure 9.8).

In the context of morphology, the principal information that is obtained from such experiments is the conformational distribution of the polymer chains. In recent years, microscopes have been developed which allow the simultaneous observation of the surface and spectroscopic examination of the surface. The illuminating beam is brought down the optical axis and the reflected light is then collected using fibre optics. The spot size is typically several tens of micrometres but can be smaller and does allow characterization of domains or phase structure that has dimensions of this order. The techniques and their application are covered in detail elsewhere.[16]

9.5 X-Ray and Neutron Diffraction Analysis[13]

One of the most interesting questions that one can ask is whether the density changes abruptly or in a gradual manner as the interface is approached.

9.5.1 Neutron and X-ray Reflectivity[21,22]

If we consider a wave impinging on an interface between two materials, refraction will occur reflecting the difference between the two refractive indices. For a strictly planar wave there will also be specular reflection (Figure 9.9).

The reflectivity is defined as the ratio of the intensities of the reflected and incident beams and should be differentiated from the reflectance which is the ratio of the amplitudes of the incident and reflected waves. The reflectance in general is a complex number because there is usually a change in phase of a wave on reflection whereas reflectivity is a real number varying from zero to unity. The specular reflection can provide information on the composition distribution normal to the surface. The reflectivity is a function of both the angle of incidence of the beam to the surface and the refractive index changes of the substrate. The reflectivity is a function of the length scale of interactions of
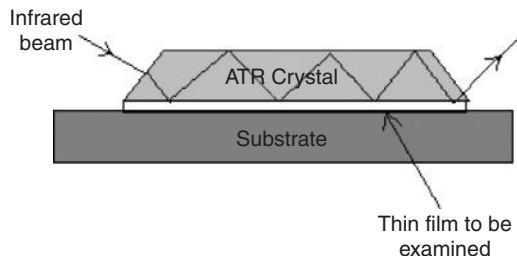
Infrared
beam

ATR Crystal

Substrate

Thin film to be
examined

Figure 9.8 Schematic of the ATR experiment. The infrared beam is guided along the
surface of the sample. The infrared beam is totally internally reflected
within the ATR crystal but probes the surface of the film to a depth that is
of the order of several micrometres. This type of experiment can be used to
provide important information of the conformational distribution in the
case of polymers. Similar experiments can be used to examine the Raman
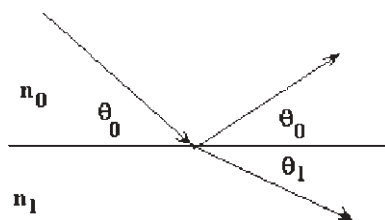and visible–UV spectra of the surface.

n_0

θ_0

θ_0

θ_1

n_1

Figure 9.9 Schematic of incident, reflected and refracted beams at an interface
between two materials with, respectively, refractive indices n_0 and n_1;
$n_1 < n_0$ and $\theta_1 < \theta_0$ which is typically the case for neutrons incident on a
material.

the wave with the surface. Visible red light from a helium–neon laser incident at
45° will have a perpendicular component of its wave vector of about 7×10^{-3}
nm, so we expect measurements of light reflectivity to be sensitive to interfacial
features at a length of ~100 nm. To probe length scales of the order of 10–100
Å requires the use of a wave with a perpendicular component of wave vector
between 0.1 and 0.01 Å. This can be achieved either using neutrons or X-rays.
Neutrons are useful in that there can be selective targeting by doping the
polymer to be studied with deuterium.

The method used parallels that for conventional optics.[22,23] Consider a plane
wave travelling in medium 0, incident on the smooth surface of medium 1
(Figure 9.10). The associated wave vectors in each medium are k_0 and k_1 and
the refractive index at the boundary is given by $n = k_1/k_0$. This refractive index
can be written as

$$n = 1 - \lambda^2 A + i\lambda C \qquad (9.18)$$

where the complex term accounts for any absorption in medium 1. For neutron
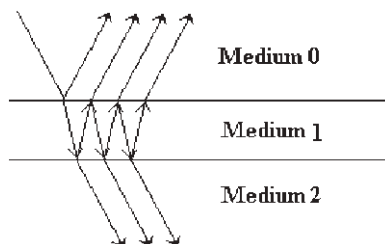beams

Figure 9.10 Multiple reflection and transmission for a beam incident on a layer of refractive index different from that of the bulk of the substrate.

$$A = \frac{Nb}{2\pi} \quad \text{and} \quad C = \frac{n\sigma_A}{4\pi} \tag{9.19}$$

where N is the atomic number density of medium 1 and b the bound atom coherent scattering length. The terms b and σ vary in an unpredictable manner across the periodic table. For the atoms occurring in most polymers, absorption cross-sections are either zero or negligible and the absorption and can be ignored in eqn (9.18). For polymeric species and solvents of low relative molar mass, Nb can be replaced by the scattering length density of the polymer segment or solvent molecule, ρ, and

$$\rho = \frac{N_A d \sum_i b_i}{m} \tag{9.20}$$

where d is the physical density of the polymer, m is the molar mass of the segment or solvent molecule and $\sum_i b_i$ is the sum of the bound atom coherent scattering length of the atoms making up the interfacial region. For X-rays similar expressions are obtained:

$$\rho = \frac{N_A d}{m} \sum_i z_i r_\rho \tag{9.21}$$

where r_ρ is the electron radius (2.82×10^{-15} m) and $\sum_i z_i$ is the sum of the electrons in the species.

At the interface between two dissimilar materials the grazing angle of incidence, θ_0, is related to the angle of reflection, θ_1, by

$$n_0 \cos \theta_0 = n_1 \cos \theta_1 \tag{9.22}$$

If medium 0 is air, then n_0 is 1 and eqn (9.22) becomes

$$\cos \theta_0 = n_1 \cos \theta_1 \tag{9.23}$$

When n_1 is less than 1 there will exist a critical angle above which the angle of reflection will be real for all incident angles. At this critical angle of incidence,

θ_c, θ_1 is zero and

$$\cos \theta_c = n_1 \tag{9.24}$$

In the case of neutron reflectivity the $\cos \theta_c$ term will be small allowing simplification of eqn (9.24) to give

$$\theta_c = \left(\frac{\lambda^2}{\pi} \rho \right)^{1/2} \tag{9.25}$$

For a smooth surface the components of the incident beam's wave vector normal to the surface are k_{z0} which is equal to $(2\pi/\lambda)\sin \theta_0$ in air and in the polymer k_{z1} is $(k_{z0}^2 - 4\pi\rho)^{1/2}$ which can also be written as $(k_{z0}^2 - k_c^2)^{1/2}$, where k_c is the value of the component of the wave vector normal to the surface at the critical angle. The reflectance of the interface between media 0 and 1 is given by the Fresnel formula:

$$r_{01} = \frac{k_{z0} - k_{z1}}{k_{z0} + k_{z1}} \tag{9.26}$$

The reflectivity R is $r_{01}r_{01}^*$, where r_{01}^* is the complex conjugate of r_{01}; hence for a smooth interface the Fresnel reflectivity is

$$R_F(Q) = \left(\frac{Q - (Q^2 - Q_c^2)^{1/2}}{Q + (Q^2 - Q_c^2)^{1/2}} \right)^2 \tag{9.27}$$

where Q is the momentum transfer normal to the surface defined as $Q = (4\pi/\lambda)\sin \theta$. If we now replace $Q_c = 4\pi^{1/2} \rho^{1/2}$ we find that when $Q \gg Q_c$ we can simplify eqn (9.27) to

$$R_F(Q) = \frac{16\pi^2\rho^2}{Q^4} \tag{9.28}$$

At high values of Q the product $Q^4R(Q)$ should become constant and have a scattering length which is determined by the bulk density of the material.

The above simplified case assumes that the refractive index/density changes abruptly at the interface. As we will see later, this need not be the case, and in practice there may be a gradual change from the value of air to the bulk values. To describe this situation the substrate may be divided into a series of layers, each of a constant but slightly different refractive index/density. To understand the analysis we shall consider the simple case of a single overlayer (Figure 9.10).

In this more complex case eqn (9.27) has the form

$$R_F(Q) = \left| \frac{r_{01} + r_{12}\exp(2i\beta)}{1 + r_{01}r_{12}\exp(2i\beta)} \right|^2 \tag{9.29}$$

where the r_{ij} terms are the Fresnel reflectances calculated for each interface and β is the phase shift or optical path length in medium 1:

$$\beta = \frac{2\pi}{\lambda} n_1 d \sin \theta_1 \tag{9.30}$$

Careful examination of the equations indicates that the reflected beam in medium 0 will be constructed from a series of beams of different path length and hence the detector will see the result of the interference between the reflected beams leading to a series of maxima and minima. The separation of the minima in Q, ΔQ, is related to the layer thickness by

$$\Delta Q = \frac{2\pi}{d} \tag{9.31}$$

Similar formulae in terms of the Fresnel reflectances may be built up for the situation with a small number of discrete layers. A larger number of layers demands the use of a more general method in which the 'surface' is considered in terms of a series of layers of slightly different characteristics. The models that are used in practice consider the density variation to be a smooth function of the distance from the surface but also may include specifically a different surface layer to account for surface roughness and the possibility of molecular segregation at the surface.

The analysis is discussed in more detail elsewhere,[13] but it takes the form proposed by Born and Wolf[23] for stratified media (Figure 9.11).

The layers in the interface (Figure 9.11) can be represented by a characteristic matrix of the form for an m-layered system:

$$M_m = \begin{bmatrix} \exp(i\beta_{m-1}) & r_m \exp(i\beta_{m-1}) \\ r_m \exp(-i\beta_{m-1}) & \exp(-i\beta_{m-1}) \end{bmatrix} \tag{9.32}$$

where β is the optical path length of layer m as defined before and r_m is the product of the Fresnel reflectance of the mth interface, $r_m{}^{f}$, and a damping term is introduced that takes account of the roughness:

$$r_m = r_m^f \exp(-0.5 Q_{m-1} Q_m \langle \sigma \rangle^2) \tag{9.33}$$

where $\langle \sigma \rangle^2$ is the mean square roughness of the interface and $Q_i = (4\pi/\lambda)\sin \theta_i$. For a total of n layers a resultant 2 by 2 matrix is obtained by multiplying these n characteristic matrices:

$$M_n = M_1 \times M_2 \times M_3 \times \cdots \times M_n \tag{9.34}$$

$$= \begin{bmatrix} M_{11} & M_{21} \\ M_{21} & M_{22} \end{bmatrix} \tag{9.35}$$

The reflectivity of the whole multilayer is then obtained as

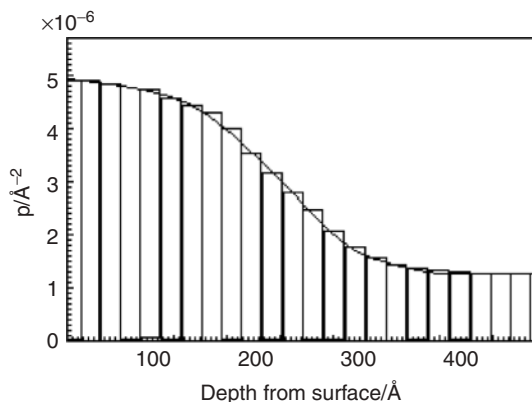$$R(Q) = \frac{M_{21} M_{21}^*}{M_{11} M_{11}^*} \tag{9.36}$$

Figure 9.11   The gradual change in scattering length density (continuous line) and its approximation as a series of discrete layers.

As indicated previously, the use of deuterium substitution allows the introduction of contrast between these doped molecules and the rest of the hydrogenated matrix. The details of such experiments are discussed elsewhere.[13]

The neutron and analogous X-ray measurements can provide density contours from the surface that can be used to understand the way in which the conformational distribution of the chains varies form the surface to the bulk. The conformational distribution defines the size of the polymer coil and hence the density of the material.

9.6   Ion Beam Analysis: Electron Recoil and Rutherford Backscattering

Another method of probing the density distribution relative to the surface is Rutherford backscattering. The principle of the method is that of scattering of a heavy particle, such as a helium ion, by the nucleus. Such events are rather infrequent but sufficiently occur to allow study of atomic distributions. Observation of the ions that are scattered back from a sample gives an indication of the distribution of the atomic density relative to the surface.[24] As with other ion probe methods, the ability of a scattered ion to escape from the surface will depend on its energy relative to an escape parameter and hence the information obtained depends on the depth of the scattering event relative to the surface. The typical depth resolution for an organic material is ~ 300 Å. This method has yet to find wide application to polymer systems and is best used to follow the distribution of heavy atomic species in a matrix of lighter material.

Forward recoil spectroscopy. This is a variant of the Rutherford backscattering method. However, rather than detecting the energy of the scattering ions it detects the recoiling target nuclei by using low grazing angles. This method has been studied more extensively for polymers because it is able to differentiate

between deuterium and hydrogen and can be used to parallel the type of doping experiments that study neutron scattering. The topic of forward recoil spectroscopy has been reviewed by Jones and Kramer[25] and will not be considered further here. The limited availability of the necessary high-energy beam sources has limited the extent to which this method has been used for the study of polymer systems. Segregation of deuterated polymer in a hydrogenated–deuterated polystyrene blend has been reported by Jones and Kramer[25] and illustrates the power of the method.

9.7 Vacuum Techniques: X-ray Photoelectron Spectroscopy (XPS), Secondary Ion Mass Spectroscopy (SIMS), Auger Electron Spectroscopy (AES)

Whilst a number of methods exist for the study of surfaces, three vacuum analysis methods have been most successfully applied to the characterization of polymer surfaces: X-ray photoelectron spectroscopy (XPS), Auger electron spectroscopy (AES) and secondary ion mass spectroscopy (SIMS).

9.7.1 X-Ray Photoelectron Spectroscopy

XPS, or as it is sometimes called electron spectroscopy for chemical analysis (ESCA), allows characterization of the elemental composition of the top 10–30 Å of a material. Its disadvantage is that it is a high-vacuum technique and hence can only be used for the study of materials whose structure is not sensitive to the application of a vacuum.

The technique involves the irradiation of the sample with a fine beam of X-rays. The X-rays ionize the core electrons, which are emitted as photoelectrons and their energy is analysed (Figure 9.12).

The incident X-ray beam has an energy given by $h\nu$, where ν is the frequency. The X-rays are able to ionize an electron from the core K shell which is emitted with an energy given by

$$E_k = h\nu - E_b - e\Phi \tag{9.37}$$

where E_k is the measured kinetic energy of the electron and E_b is the binding energy of the core electron state. The X-ray source will be typically an Mg K_α source with an energy of 1253.6 eV or an Al K_α source with an energy of 1486.5 eV. A correction for the energy involved in the electron escaping from the surface is required: this is designated $e\Phi$, its precise value being dependent on the sample and spectrometer. Since all samples will contain carbon as a contaminant, it is usual to calibrate the energy by adjusting the values to the accepted values of carbon, 285.0 eV.
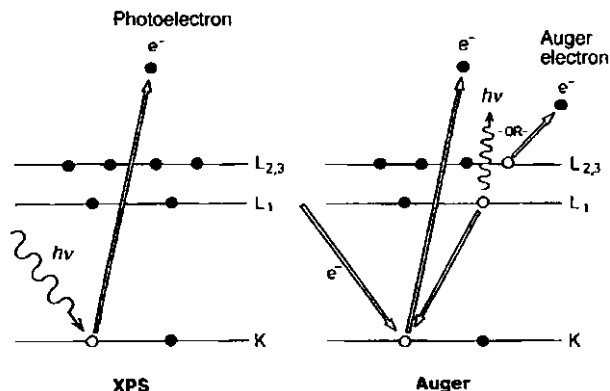
Figure 9.12   Schematic showing X-ray photoelectron and Auger processes.

Table 9.3   Binding energies and shifts for atomic species commonly encoun-
tered in polymers.

	Binding energy (eV)					
Element	$1s_{1/2}$	$2s_{1/2}$	$2p_{1/2}$	$2p_{3/2}$	$3s_{1/2}$	$3p_{3/2}$
Hydrogen	14					
Boron	188		5			
Carbon	284		7			
Nitrogen	399		9			
Oxygen	532	24	7			
Fluorine	686	31	9			
Sodium	1072	63	31			
Aluminium		118	74	73		
Silicon		149	100	99	8	3
Phosphorus		189	136	135	16	10
Sulfur		229	165	164	16	8
Chlorine		270	202	200	18	7

Each element has a distinct set of binding energies that are characteristic of that atom (Table 9.3).

Photoelectrons are labelled according to the principal quantum numbers (n) with values 1, 2, 3, 4, 5 or 6 and the angular quantum numbers with values of 0, 1, 2 or 3 commonly designated by the letters s, p, d and f. Doublets are present in the non s level as a result of spin orbital coupling. Two possible states exist and are specified by the quantum number ($j = l \pm s$, where s is the spin quantum number), when l exceeds 0. For example, a 2p level has a doublet designated by $2p_{1/2}$ and $2p_{3/2}$ and a 3d core level has a doublet designated by $3d_{3/2}$ and $3d_{5/2}$. After a photoelectron has been ejected from an inner shell of an atom, the excited atom can relax by one of two mechanisms. The hole created by the ejection of the photoelectron can be filled by an electron from an outer shell, releasing an amount of energy that can be emitted as a quantum of X-ray radiation; or the energy can be given to another electron in the same level or

lower level (Figure 9.12). In Section 9.3.2.2, these emitted X-rays were discussed as regards EDAX for element identification. If an electron is ejected from the $L_{2,3}$ shell then this Auger electron is then emitted with a kinetic energy approximately given by

$$E_k = E(K) - E(L_1) - E(L_{2,3}) \qquad (9.38)$$

where $E(K)$, $E(L_1)$ and $E(L_{2,3})$ are the atomic energy levels. The two processes mentioned above are called X-ray fluorescence and Auger emission, respectively. For low atomic number elements ($Z < 30$), Auger emission tends to be the dominant process. Thus, in an XPS spectrum, Auger electron peaks also appear and occasionally overlap with photoelectron peaks. The kinetic energy of Auger electrons is characteristic of the elemental composition and is independent of the excitation energy, while the kinetic energy of the photoelectrons depends on the X-ray energy.

Clark and co-workers[26] using pure polymers and model compounds have reported a number of values that can be used as reference data. Some typical values for groups encountered in polymer science are listed in Table 9.4.

Subtle interactions between the nucleus and the core levels produce small but measurable *chemical shifts*. The chemical shifts vary from 1 eV for Br, to 1.5 eV for Cl to about 2.9 eV for F. A shift of as much as 8.5 eV has been observed for a $-CF_3$ moiety in a polyimide. The effect of oxygen that is conjugated to the carbon can lead to significant shifts: 3.8 eV in a polyimide. An example of the type of spectrum obtained for a polymeric material is shown in Figure 9.13 for PF6MA.[27]

The deconvolution of the spectrum is carried out on the basis of the peaks having an approximate Gaussian shape and adjusting the peaks to recognized shifts. Because of the large shifts produced by fluorine substitution, polymers either containing fluorine or modified as a result of being exposed to fluorine plasma or reactions have been extensively studied. As expected the incorporation of fluorine lowers the surface energy. The primary effect of nitrogen functionalities varies with the substituent and C 1s shifts of 0.2, 0.6, 1.8 and 1.8 eV are obtained for $-N(CH_3)_2$, $-NH_2$, $-NCO$ and NO_2, respectively. C 1s in $-C\equiv N$ exhibits a shift of 1.4 eV.

An example of the use of deconvolution to study poly(vinyl alcohol) (PVA) adsorbed on poly(vinylidene fluoride) (PVDF) is shown in Figure 9.14. PVA is obtained from poly(vinyl acetate) and the hydrolysis process can leave a residual low content of the acetate in the polymer. The spectrum of the virgin PVDF is shown as the dotted curve in Figure 9.14. This spectrum demonstrates that in ideal conditions quantities of the order of 1% can be detected.

Secondary spectral features such as shake up satellites are frequently observed for polymeric materials containing unsaturated hydrocarbons. Theoretical studies have shown that these are associated with π–π^* transitions in aromatic materials. The shake up peak is clearly visible in the spectra of an oligomeric polyalkylthiophene that is being subjected to attack by O_3[29] and polystyrene[28] (Figure 9.15). It should be noted that the difference between the binding energy for aliphatic carbons in the backbone of polystyrene and the

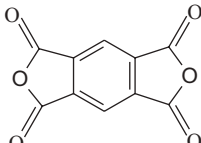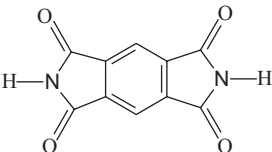**Table 9.4**   Examples of chemical shifts for some polymer entities.

Group	Structure	Lowest peak (eV)
Polyethylene		284.8 (C_{1s})
Polypropylene		284.9 (C_{1s})
Poly(vinyl chloride)		286.5 (C_{1s})
Poly(vinyl bromide)		286.5 (C_{1s})
Polytetrafluoroethylene		292.0 (C_{1s})
Polystyrene		284.2 (C_{1s})
Pyromellitic acid dianhydride		286.9 (C_{1s})

Table 9.4 (*continued*)

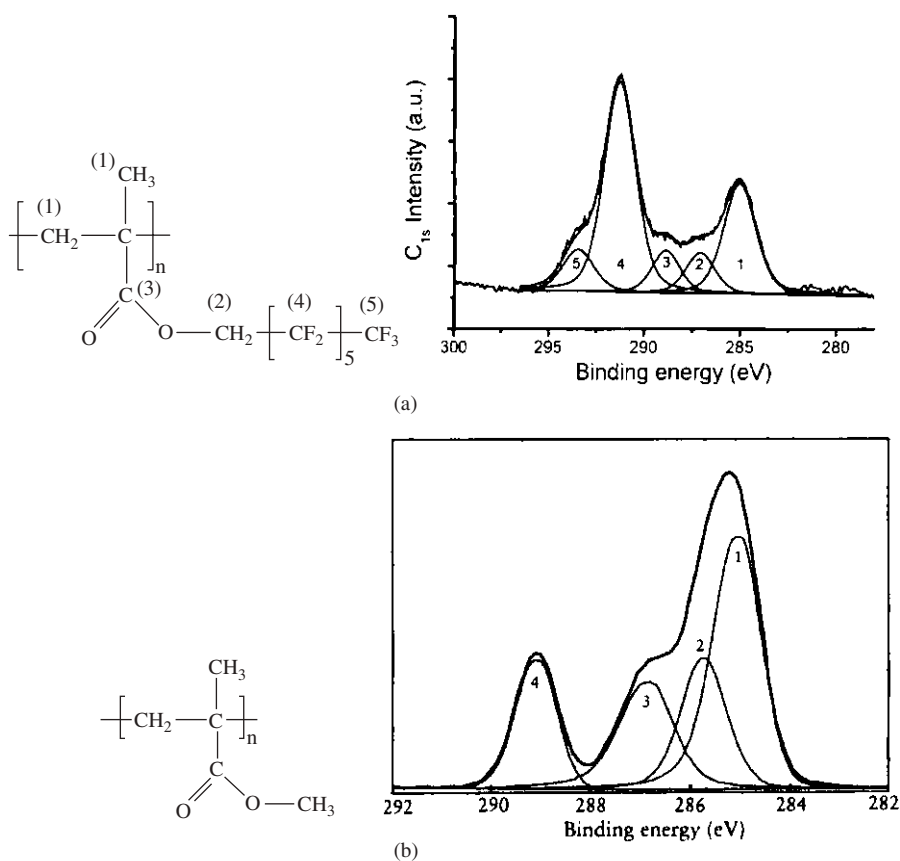| Group	Structure	Lowest peak (eV)
Pyromellitic diimide		285.7 (C_{1s})

(a)

(b)

Figure 9.13 Structure and XPS traces of the C_{1s} region showing the carbon atoms in different environments: (a) PF6MA; $-CH_x-C-$ (1), $-CH_2O$ (2), $-CF_2-$ (4), $-CF_3$ (5);[27] (b) poly(methyl methacrylate) obtained using an Al K_α source allowing higher resolution.[28]
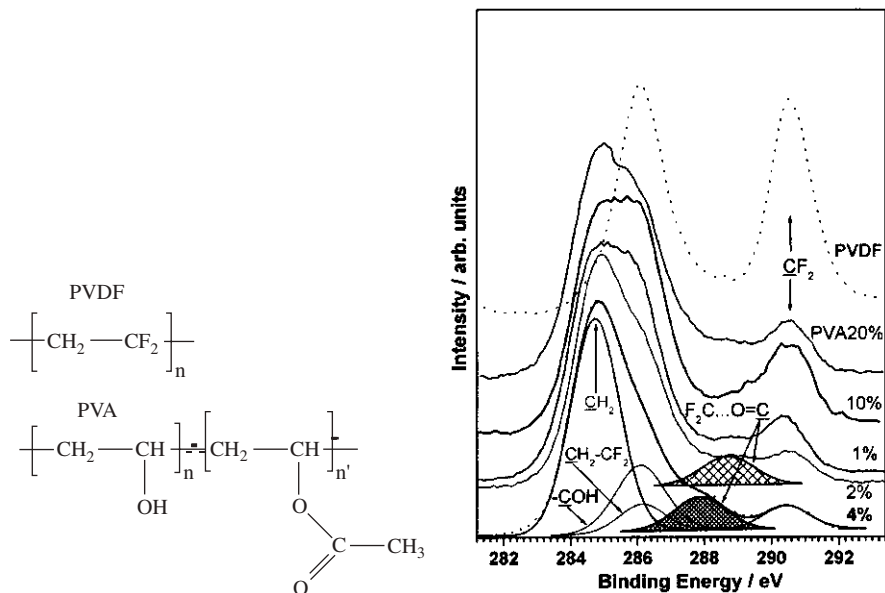
Figure 9.14   Carbon 1s spectra for virgin PVDF and 4% PVA adsorbed on the PVDF surface.[29]

ring carbons is very small making identification of the polymer difficult. The intensity of the satellite as a function of the main photoelectron peak is constant at about 10%, although slight changes occur depending on the structure of the polymer involved. The shake up peak provides a quantitative way in which the surface concentration of phenyl groups following a particular treatment method may be estimated. The peak also provides a means of estimating surface modification brought about by ring opening reactions.

The O 1s and N 1s both vary in a narrow range of about 2 eV at about 533 and 399 eV, respectively. Oxidized nitrogen functions, however, exhibit much higher N 1s binding energies that vary from 405 to 408 eV for a change from –ONO to –ONO$_2$.

9.7.2   Electron Mean Free Path, Attenuation and Escape Depth

In order to be able to analyse the spectra it is important to understand the location of the atoms that are giving rise to the events being observed. For XPS and Auger techniques the electron that is being measured must be detected without it undergoing significant interaction with the polymer material through which it is moving. As it moves through the polymer it is capable of undergoing inelastic interactions leading to ionization or excitation of valence and inner electrons, as well as vibrational excitations. Photoelectrons suffer loss of kinetic energy as a result of inelastic scattering. This limits the non-loss emission to a mean depth of only a few atomic layers below the surface and thus makes this
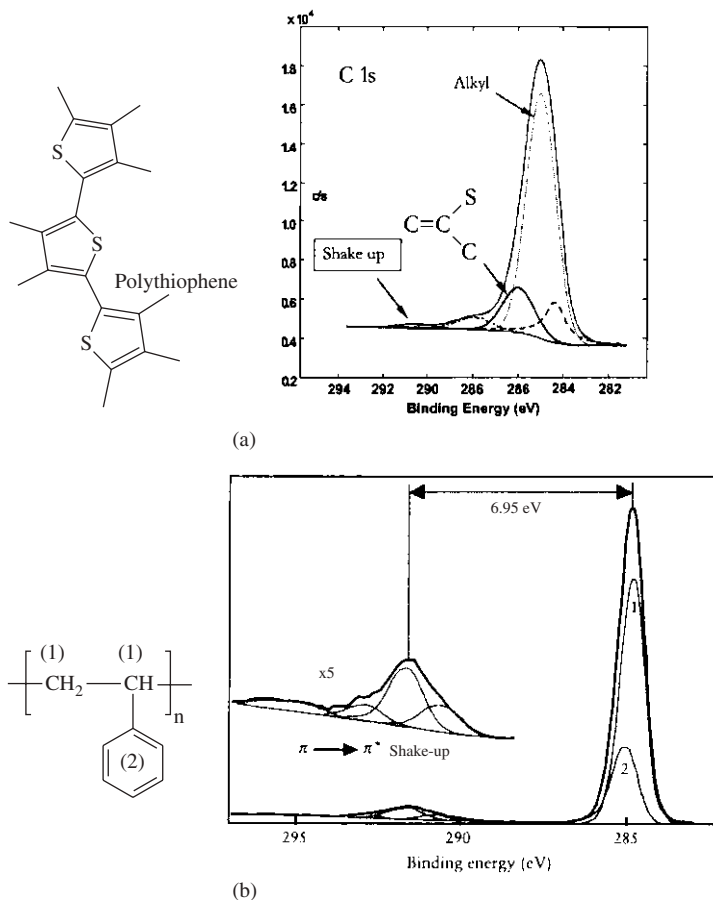
(a)

(b)

Figure 9.15 Fitted C 1s spectrum of polythiophene[30] (a) and polystyrene (b). In both XPS spectra the shake up peak is visible at ~ 6.95 eV above the C 1s peak.

technique surface sensitive. The intensity of the photoelectrons that suffer no loss in kinetic energy after travelling a distance z is found to follow an exponential decay law:

$$I(z) = I(i) \exp\left(\frac{-z}{\lambda_a(E_k)\cos\theta}\right) \qquad (9.39)$$

where $I(i)$ is the initial intensity of the photoelectron flux generated at a given point in the solid, $\lambda_a(E_k)$ is the attenuation length of the photoelectron with kinetic energy E_k, θ is the angle between the direction of the emitted photoelectrons to the analyser and the surface normal and z is the distance measured from the event to the surface (Figure 9.16). For a semi-infinite sample, the photoelectron intensity I^∞ can be obtained by integrating eqn (9.39) from $z = 0$
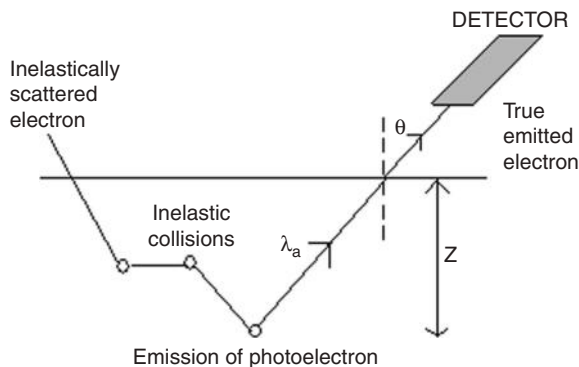
Figure 9.16 Schematic showing the photoelectron trajectories after creation.

to $z = \infty$. The terms *inelastic mean free path*, *attenuation length* and *escape depth* are used. The problem of the mean free path has been extensively investigated and it is found that it follows a 'universal curve'[31] (Figure 9.17). The mean free path reaches a minimum at between 20 and 50 eV.

The variation of the mean free path with electron energy E_k can be described by an equation that has the form

$$\lambda_a(E_k) = \frac{538 a_A}{E_k^2} + 0.41 a_A (a_A E_k)^{0.5} \tag{9.40}$$

where E_k is the energy of the photoelectron in eV, a_A^3 is the volume of the atom in nm^3 and λ_a is in nm. For many solids the following alternative relationship has been found to be useful:

$$\lambda_a(E_k) = \frac{(49 E_k^{-2} + 0.11 E_k^{0.5})}{\rho} \tag{9.41}$$

where ρ is the density of the material in g cm^{-3}.

In XPS a method of determining the attenuation length is to use the overlayer method. The variation of the intensity of a species is determined as a function of the thickness of the overlayer. If the substrate is a silicon wafer and the overlayer has a thickness d, then the intensity of the silicon signal will be I_s, which according to eqn (9.39) is given by

$$I_s = I_s^\infty \exp\left(\frac{-d}{\lambda_a^s \cos\theta}\right) \tag{9.42}$$

where λ_a^s is the attenuation length for the photoelectron generated in the substrate. The photoelectron intensity for the overlayer is given by
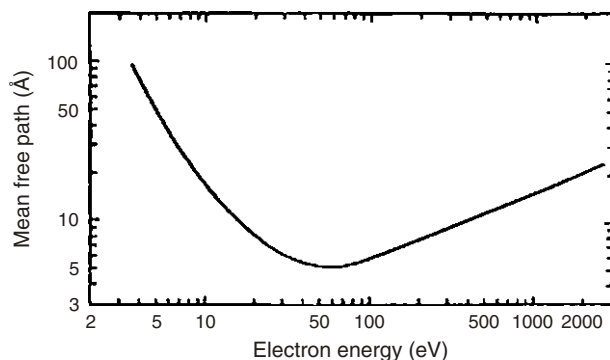
Figure 9.17 The 'universal curve' for the mean free path as a function of the electron kinetic energy according to eqn (9.40)

Table 9.5 Escape depths for some common elements with Mg K_α and Al K_α.

Element	Core level	Kinetic energy (eV) Mg K_α	λ_k (nm)	Kinetic energy (eV) Al K_α	λ_k (nm)
F	1s	568	2.0	3825	5.2
O	1s	722	2.3	3979	5.3
N	1s	855	2.5	4112	5.4
C	1s	970	2.6	4227	5.5
Si	1s	1105	2.8	4362	5.6
F	2s	1223	3.0	4480	5.7
O	2s	1230	3.0	4487	5.7

$$I_0 = I_0^i \int_d^0 \exp\left(\frac{-z}{\lambda_a^0 \cos\theta}\right) \partial z \qquad (9.43)$$

$$= I_0^i \lambda_a^0 \cos\theta \left[1 - \exp\left(\frac{-d}{\lambda_a^0 \cos\theta}\right)\right] \qquad (9.44)$$

$$= I_0^\infty \left[1 - \exp\left(\frac{-d}{\lambda_a^0 \cos\theta}\right)\right] \qquad (9.45)$$

where I_s^∞ and I_s^0 are the photoelectron intensities of the pure substrate and the overlayer at infinite thickness, respectively. Examples of typical values for some common elements are listed in Table 9.5.

In the context of surfaces it is interesting to note that changing from Mg K_α to Al K_α almost doubles the escape depth and hence allows the distribution of elements to be studied deeper into the surface.
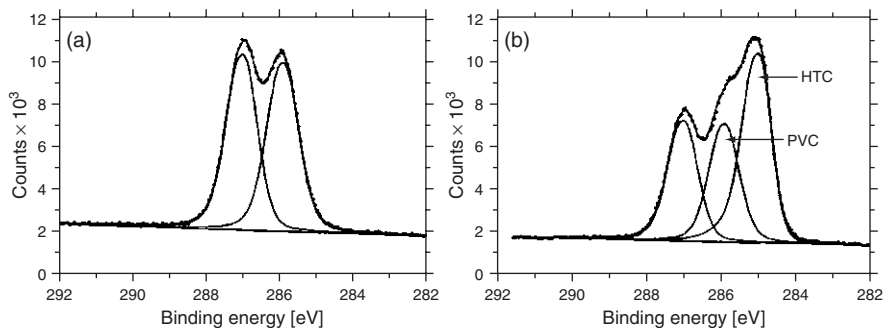
Figure 9.18 C 1s spectra of (a) poly(vinyl chloride) (PVC) and (b) PVC contaminated with hexatriacontane (HTC).[42]

The surface sensitivity of XPS is illustrated by comparison of the spectra of a clean surface and one contaminated with hexatriacontane (Figure 9.18). The presence of the contamination at the polymer surface is easily identified.[42]

9.7.3 XPS Depth Profiling

The normal application of XPS will give information on the atomic composition over the entire sampling depth. It is useful to be able to explore whether surface segregation may be occurring and for this to be achieved it is appropriate to use the escape depth as a tool for the analysis of different depths.

Angular resolution XPS. Inherent in eqn (9.42) is the angle of the emission θ of the photoelectron. The escape depth is defined as the distance normal to the surface at which the probability of an electron escaping without significant energy loss due to the inelastic scattering process drops to e^{-1} of its original value. The escape depth is given by

$$\zeta = \lambda_a \cos \theta \tag{9.46}$$

where ζ is the escape depth, λ_a is the attenuation length and θ is the angle of emission. A specimen recorded at $\theta = 0°$ will have the maximum sample depth, which is twice the sampling depth of a spectrum recorded at a value of $\theta = 60°$. The angular dependence studies are the most frequently used non-destructive approach to depth sampling. The mean depth below the surface from which the photoemissions occur can be described by[32]

$$d = 3\lambda_a \sin \theta_2 \tag{9.47}$$

where d is the depth and θ_2 is the angle between the surface and the take off angle which is the complement of θ as defined in Figure 9.16. The value of λ depends on E_k^x, where typically $0.5 < x < 1$. Some typical values determined using poly(methyl methacrylate) are listed in Table 9.6.

Different X-ray energies. As indicated in Table 9.5, the escape depth is a function of the photoelectron energy. This is illustrated by a study of surface

Table 9.6 XPS sampling depths as a function of core kinetic energy and take off angle.

| | *Kinetic energy (eV)* | | *Sampling depth (nm)* | | | | | |
| | | | *Mg K$_\alpha$* | | | *Al K$_\alpha$* | | |
Core level	*Mg K$_\alpha$*	*Al K$_\alpha$*	*10°*	*45°*	*90°*	*10°*	*45°*	*90°*
F 1s	568	801	0.8	3.4	4.8	1.1	4.5	6.3
O 1s	723	956	1	4.1	5.8	1.3	5.2	7.3
N 1s	852	1185	1.1	4.7	6.6	1.4	5.7	8
C 1s	967	1200	1.3	5.2	7.3	1.5	6.2	8.7
Si 1s	1152	1385	1.5	5.9	8.4	1.7	6.9	9.7

Table 9.7 Angle and source dependence showing atomic ratios for a study of segmented polyurethanes.

| | *Ratio* | | | | |
Anode	*C/O*	*N/C*	*N/O*	*Angle of emission (°)*	*Depth (nm)*
Mg	4.0	0.04	0.15	75	2.7
Mg	4.0	0.04	0.17	45	7.3
Mg	4.0	0.05	0.19	0	10.3
Ti	4.0	0.07	0.32	0	21.5

segregation in segmented poly(ether-urethane) block copolymers.[33] The molecular structure of the polymer is similar to that shown in Figure (8.13) has the form
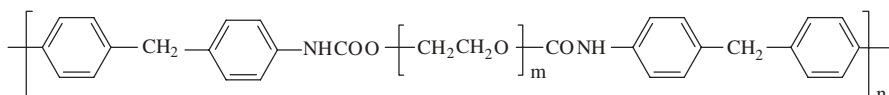
The urethane linkage is hydrogen bonded with other urethanes and being part of the methylene diphenyl entity forms a phase separated entity which melts at ~158°C and is termed the 'hard' block. Examination of the chemical structure indicates that the nitrogen will be incorporated only in the hard block and hence is an indicator of its location in the material. If in addition to looking at different angles, sources with different energies are used, a range of different sample depths can be explored (Table 9.7).

If there were no segregation of the hard segments then the atomic ratios should be independent of the angle and the source used. Segregation of the soft block at the surface will be detected as an increase in the N/C and N/O ratios with an increasing sampling depth. The data in Table 9.7 indicate that the polyether is preferentially segregated at the surface. This segregation is important in certain applications. This type of polyurethane is used in blood handling equipment and the compatibility of the materials with blood is critical to avoid damaging blood cells and inducing thrombosis. The segregated polyether can be easily hydrated by the blood and forms a 'soft' interface that minimizes

damage. Table 9.7 illustrates that the angular and energy variation allows exploration of depths between 2 and 22 nm.

Sputtering. For analysis of thicker films destructive methods have to be used. For inorganic materials bombarding the surface with a heavy ion, such as argon, allows the slow removal of the surface and exposure of sublayers. In the case of organic and other covalently bonded materials this approach is not very helpful since the species that are created may not be representative of the original material.

9.7.4 Secondary Ion Mass Spectrometry (SIMS)

In the context of XPS ion bombardment of a polymer was not considered appropriate; however, if carefully controlled and supported with appropriate analytical techniques it is a very useful method for surface analysis. In SIMS two processes have to be considered: sputtering (emission of particles) and ionization of particles (Figure 9.19).

At low incident ion flux single events may occur (Figure 9.19a); however, as the beam flux is increased then multiple events must be considered to become more frequent (Figure 9.19b). The single knock off regime is associated with ion beams of less than 1 keV, the energy transferred to the target being only capable of producing primary recoil events. Atoms from the target are ejected if they have sufficient energy to overcome the surface binding energy. The linear cascade regime occurs at slightly higher energy where now the impact of the incident ion is able not only to produce ejection of ions but is also able to transfer sufficient energy to the surface to induce secondary ionization. The incident ions used are often Ar^+ or Xe^+ ions; for high resolution Ga, In, Sn, Au and Cs ions have been used. A number of theoretical models have been produced which attempt to model the processes occurring; however, these have only a limited success. The important features to recognize are:

- The incident ion can produce the ejection of a neutral particle but also can eject ions. The accumulation of Ar^+ ions will lead to the surface becoming charged.
- If the surface becomes positively charged it will influence the energy that the incoming ion will have and is able to transfer to the substrate.
- If a negative ion is ejected this will increase the positive charge at the surface. Unless this residual charge is neutralized it will affect the surface
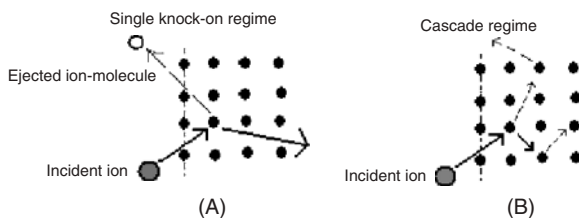

**Figure 9.19**   Schematic of the SIMS process.

energy and hence the ability of subsequent ions to be ejected. It is common to use an electron gun to flood the surface. This neutralizes the charges that are trapped in the surface.

- Secondary interactions due to multiple collisions will assist the fragmentation of the molecules and as the molar mass is reduced so their ability to leave the surface will increase.
- The ejected ions will have been generated in the topmost layers and rarely will have come from a distance of more than 1 nm from the surface.

The SIMS spectrometer is simply a source of mono-energetic and collimated ions that are targeted at a surface that is contained in a vacuum. The ejected ions are then carefully collected and their molar mass analysed. The ability to differentiate between different species will depend on knowledge of the fragmentation pattern or the ability to identify a unique ion that can be associated with a particular structure.

Briggs and co-workers[34–39] have reported spectra for a range of polymer systems. A typical problem might be the differentiation of polyethylene, polypropylene and polyisobutylene (Figure 9.20). The species that are ejected will be composed of both positive and negative ions. The ions are collected by the use of an accelerating voltage that can be either positive of negative relative to the sample. Depending on the sign of the collecting voltage, the spectrum of the collected species will change. In practice most measurements are made collecting the positive charges; however, in certain cases examination of the negative ion spectrum can significantly help identification of species.

Although there are a number of mass peaks for each polymer, the assignment of particular peaks to a unique species can sometimes be difficult. It is possible that a particular atomic mass unit (amu) can arise from different species. In the spectra in Figure 9.20 the 69 amu peak is assigned to a dimethyl-cyclopropyllium ion:
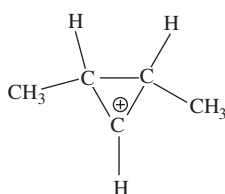
which can be formed by a rearrangement of the fragmentation products of the chain. The 69 amu peak is strongest in polypropylene but is also present in other polymers.

Other fragments that have been identified are:
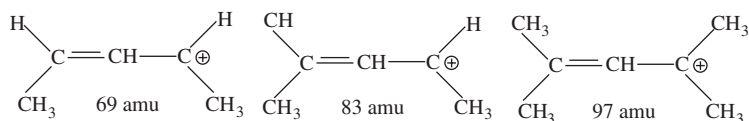
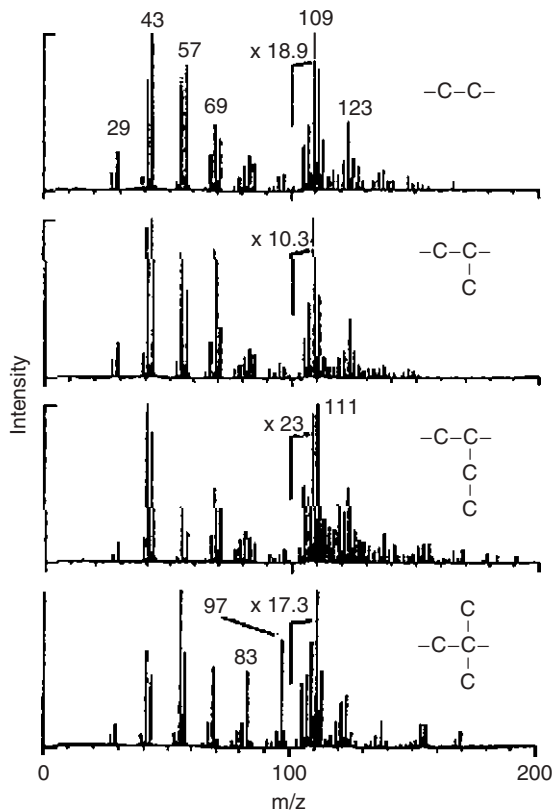The allyl structure is the more likely assignment for the 69 amu ion.

Figure 9.20   Positive ion spectra of (top to bottom) low-density polyethylene, poly-propylene, poly(but-1-ene) and polyisobutylene.
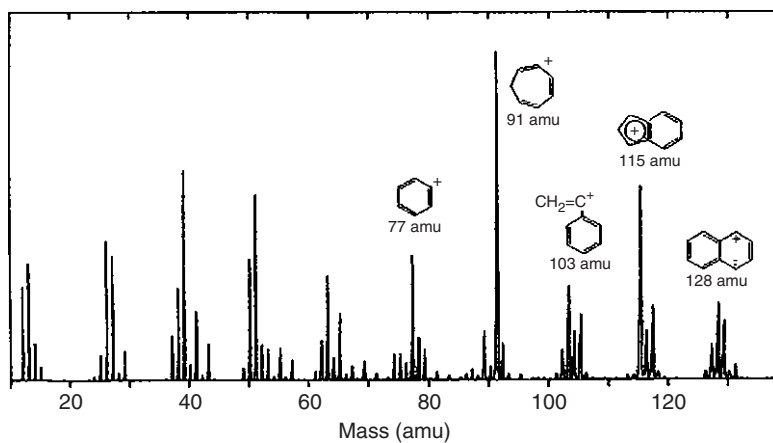

Figure 9.21   Positive ion SIMS spectrum of polystyrene.

Table 9.8 Sources of information on polymer characterization.

Technique	Reference
X-Ray diffraction	I. H. Hall (ed.), *Structure of Crystalline Polymers*, Elsevier Applied Science, London, 1984.
	B. D. Cullity, *Elements of X-ray Diffraction*, Addison Wesley, Reading, MA, 1978.
	F. J. Balta-Celleja and C. G. Vonk, *X-ray Scattering of Synthetic Polymers*, Elsevier, Amsterdam, 1989.
	L. T. Nguyen, in *New Characterization Techniques for Thin Polymer Films*, ed. H. M. Tong and L. T. Nguyen, Wiley, New York, 1990, p. 57.
Neutron diffraction	S. W. Lovesay, *Theory of Neutron Scattering from Condensed Matter*, Oxford University Press, Oxford, 1984, vol. 1.
	J. S. Higgins and H. C. Benoit, *Polymers and Neutron Scattering*, Oxford Science Publications, Oxford, 1994.
	R. A. L. Jones and R. W. Richards, *Polymers at Surfaces and Interfaces*, Cambridge University Press, Cambridge, 1999, p. 94.
Electron diffraction	D. Campbell, R. A. Pethrick and J. R. White, *Polymer Characterization Physical Techniques*, Stanley Thornes, Cheltenham, UK, 2000, ch. 9.
Transmission electron microscopy	D. B. Williams, *Practical Analytical Electron Microscopy in Materials Sciences*, Verlag Chemie International, 1984.
	E. L. Thomas, in *Structure of Crystalline Polymers*, ed. I. H. Hall, Elsevier Applied Science, London, 1984, ch. 3.
	D. Campbell, R. A. Pethrick and J. R. White, *Polymer Characterization Physical Techniques*, Stanley Thornes, Cheltenham, UK, 2000, ch. 9.
Scanning electron microscopy	D. B. Williams, *Practical Analytical Electron Microscopy in Materials Sciences*, Verlag Chemie International, 1984.
	D. Campbell, R. A. Pethrick and J. R. White, *Polymer Characterization Physical Techniques*, Stanley Thornes, Cheltenham, UK, 2000, ch. 10.
Optical microscopy	D. A. Hemsley, *Applied Polymer Light Microscopy*, Elsevier Applied Science, London/New York, 1989.
	D. Campbell, R. A. Pethrick and J. R. White, *Polymer Characterization Physical Techniques*, Stanley Thornes, Cheltenham, UK, 2000, ch. 11.
X-Ray photoelectron spectroscopy	D. Briggs, in *Electron Spectroscopy: Theory, Techniques and Application*, ed. C. R. Brundle and A. D. Baker, Academic Press, London, 1979, vol. 3.
	K. Okuno, S. Tomita and A. Ishitani, in *Secondary Ion Mass Spectroscopy SIMS IV*, ed. A. Benninghoven, Springer Series in Chemical Physics, 1984, vol. 36, p. 392.
	D. Briggs, *Surface Analysis of Polymers by XPS and Static SIMS*, Cambridge University Press, Cambridge, 1998.
	R. Scruby, *Mater. World*, 2002, **10**(6), 26.
Secondary ion mass spectroscopy	N. J. Chou, in *New Characterization Techniques for Thin Polymer Films*, ed. H. M. Tong and L. T. Nguyen, Wiley, New York, 1990, p. 289.
	D. Briggs, *Surface Analysis of Polymers by XPS and Static SIMS*, Cambridge University Press, Cambridge, 1998.

Table 9.8 (*continued*)

Technique	Reference
	K. Okuno, S. Tomita and A. Ishitani, in *Secondary Ion Mass Spectroscopy SIMS IV*, ed. A. Benninghoven, Springer Series in Chemical Physics, 1984, vol. 36, p. 392.
Atomic force microscopy	D. H. Reneker, in *New Characterization Techniques for Thin Polymer Films*, ed. H. M. Tong and L. T. Nguyen, Wiley, New York, 1990, p. 327.
Scanning tunnelling microscopy	D. H. Reneker, in *New Characterization Techniques for Thin Polymer Films*, ed. H. M. Tong and L. T. Nguyen, Wiley, New York, 1990, p. 328.

Studies of aromatic-containing polymers, such as polystyrene, indicate that rearrangement of the fragments of the polymer occurs very quickly to form stable ions (Figure 9.21). The most intense peak in the spectrum has a mass of 91 amu and is assigned to the tropyllium cation, $C_7H_7^+$. Other characteristic peaks are at 51 amu ($C_4H_3^+$), 63 amu ($C_5H_3^+$), 65 amu ($C_5H_5^+$), 77 amu ($C_6H_5^+$), 103 amu ($C_8H_7^+$) and 115 amu ($C_9H_7^+$). The important feature to appreciate is that the most obvious fragment from the polymer degradation, $C_6H_5^+$, is not the strongest peak and it is apparent that fragmentation probably involves splitting off of a vinyl-substituted phenyl ion similar to 1034 amu ($C_8H_7^+$) which then rapidly rearranges to form either the stable 91 amu tropyllium cation ($C_7H_7^+$) or by loss of another fragment forms the 65 amu phenyl cation ($C_5H_5^+$). Many papers have been published attempting to sort out the fragmentation patterns for even the simplest polymers. The usual approach that is adopted is to measure the spectrum of the pure component polymers and to use these to carry out subsequent analysis of surface segregation or analysis of blends.

The important difference between XPS and SIMS is the extreme surface sensitivity of SIMS that looks at the topmost layer of the material. It is often found that SIMS studies are very sensitive to contamination and that a monolayer of contaminant may have to be removed before assessment of a surface can be carried out.

The techniques described above are able to provide researchers with the ability to visualize the surface and also to determine quantitatively the atomic composition of both the top layer and the volume close to the surface.

9.8 Fourier Transform Infrared (FTIR) Imaging[40]

The ability to differentiate both spatially and chemically is achievable through coupling FTIR with spatially resolved infrared detectors (FPA).[41] FPA detectors typically have 4096 small detectors arranged in a 64×60 grid. The spatial resolution of the system is limited only by diffraction and is of the order of 4–10 μm depending on the wavelength of the band being imaged. By selection of an infrared absorption band specific to a particular polymer, it is possible to create a map of the distribution of that species in the surface. In blends and

similar systems the morphological features are sufficiently large to allow differentiation using this method, and systems such as polystyrene/low-density polyethylene have been reported.[40]

It is impossible in a single text to cover comprehensively the topic of polymer characterization. A list of useful references is included in Table 9.8.

Recommended Reading

D. Briggs, *Surface Analysis of Polymers by XPS and Static SIMS*, Cambridge University Press, Cambridge, 1998.
R.A.L. Jones and R.W. Richards, *Polymers at Surfaces and Interfaces*, Cambridge University Press, Cambridge, 1999.
J.E. Watts and J. Wolstenholme, *An Introduction to Surface Analysis by XPS and AES*, Wiley, Chichester, UK, 2003.

References

1. J.E. Watts and J. Wolstenholme, *An Introduction to Surface Analysis by XPS and AES*, Wiley, Chichester, UK, 2003.
2. D.R. Randell and W. Neagle, *Surface Analysis Techniques and Applications*, Royal Society of Chemistry, 1990.
3. F. Garbassi, M. Morra and E. Occhiello, *Polymer Surfaces*, John Wiley, Chichester, UK, 1996.
4. S. Wu, *Polymer Interfaces and Adhesion*, Marcel Dekker, New York, 1982.
5. D. Briggs, *Surface Analysis of Polymers by XPS and Static SIMS*, Cambridge University Press, Cambridge, 1998.
6. E.M. McCash, *Surface Chemistry*, Oxford University Press, 2002.
7. G.T. Barnes and I.R. Gentle, *Interfacial Science*, Oxford University Press, 2005.
8. J. Goodwin, *Colloids and Interfaces with Surfactants and Polymers*, Wiley, 2004.
9. D.B. Williams, *Practical Analytical Electron Microscopy in Materials Science*, Verlag Chemie International, 1984.
10. C.M. Chan, *Polymer Surface Modification and Characterization*, Hanser, New York, 1994.
11. B. Cherry, *Polymer Surfaces*, Cambridge University Press, Cambridge, 1981.
12. H.M. Tong and L.T. Nguyem, *New Characterization Techniques for Thin Polymer Films*, SPE Monograph Series, Wiley, New York, 1990.
13. R.A.L. Jones and R.W. Richards, *Polymers at Surfaces and Interfaces*, Cambridge University Press, Cambridge, 1999.
14. I.H. Hall, *Structure of Crystalline Polymers*, Elsevier Applied Science, London, 1984.
15. R.N. Wenzel, *Ind. Eng. Chem.*, 1936, **28**, 988.

16. D. Campbell, R.A. Pethrick and J.R. White, *Polymer Characterization: Physical Techniques*, Stanley Thornes, Cheltenham, UK, 2000, ch. 11.
17. F.S. Baker, J.P. Craven and A.M. Donald, in *Techniques for Polymer Organisation and Morphology Characterisation*, ed. R.A. Pethrick and C. Viney, Wiley, 2003.
18. D.C. Bassett, R.H. Olley and A.S. Vaughan, in *Techniques for Polymer Organisation and Morphology Characterisation*, ed. R.A. Pethrick and C. Viney, Wiley, 2003.
19. D.H. Reneker, *New Characterization Techniques for Thin Polymer Films*, ed. H.M. Tong and L.T. Nguyem, SPE Monograph Series, Wiley, New York, 1990, ch. 12.
20. J.K. Gimzewske, E. Stroll, Schlittler, *Surf. Sci.*, 1987, **181**, 267.
21. T.P. Russel, *Mater. Sci. Rep.*, 1990, **5**, 171.
22. R.K. Thomas, in *Scattering Methods in Polymer Science*, ed. R.W. Richards, Ellis Horwood, London, 1995.
23. M. Born and E. Wolf, *Principles of Optics*, Pergamon Press, Oxford, 1975.
24. W.K. Chu and J.W. Mayer, *Backscattering Spectroscopy*, Academic Press, New York, 1978.
25. R.A.L. Jones and E.J. Kramer, *Phys. Rev. Lett.*, 1989, **62**, 280.
26. D.T. Clark and A. Harrison, *J. Polym. Sci., Polym. Chem.*, 1981, **17**, 957.
27. R.D. Van de Grample, W. Ming, A. Gildenfenning, W.J.H. van Gennip, J. Laven, J.W. Nieantsverdriet, H.H. Brogersma, G. de With and R. van der Linde, *Langmuir*, 2004, **20**, 6344.
28. G. Beamson and D. Briggs, *High Resolution XPS of Organic Polymers*, John Wiley, Chichester, UK, 1992, p. 119.
29. S.G. Gholap, M.V. Badioger and C.S. Gopinath, *J. Phys. Chem. B*, 2005, **109**, 13941.
30. J. Heeg, C. Kramer, M. Wolter, S. Michaelis, W. Plieth and W. J. Fischer, *Appl. Surf. Sci.*, 2001, **180**, 36.
31. M.P. Seah and W.A. Dench, *Surf. Interf. Anal.*, 1970, **1**, 2.
32. D. Briggs, *Encyclopaedia of Polymer Science and Technology*, John Wiley, Chichester, UK, 2002.
33. T.G. Vargo and J.A. Gardella, *J. Vac. Sci. Technol.*, 1989, **A7**, 1733.
34. D. Briggs, *Surf. Interf. Anal.*, 1982, **4**, 151.
35. M.J. Hearn and D. Briggs, *Surf. Interf. Anal.*, 1988, **11**, 198.
36. D. Briggs, *Surf. Interf. Anal.*, 1990, **15**, 734.
37. D. Briggs, *Br. Polym. J.*, 1989, **21**, 3.
38. D. Briggs, *in Encyclopaedia of Polymer Science*, Wiley, New York, 1988, vol. 16, p. 399.
39. D. Briggs, *Surface Analysis of Polymers by XPS and Static SIMS*, Cambridge University Press, Cambridge, 1998.
40. R. Bhargava, S.Q. Wand and J.L. Koenig, *Macromolecules*, 1999, **32**, 2748.
41. R. Scruby, *Mater. World*, 2002, **10**(6), 26.
42. G. Beamson and D. Briggs, *Mol. Phys.*, 1992, **76**, 919.

CHAPTER 10
Polymer Surfaces and Interfaces

10.1   Introduction

In Chapter 9 the techniques which can be used for the study of molecular interfaces were considered and provide us with the tools to ask the question 'What are the factors that make definition of the surface difficult?' In order to help our consideration of the answer it is appropriate to divide the discussion into three types of system: crystalline polymers, amorphous polymers and polymer blends.

10.1.1   Crystalline Polymers

A bulk crystalline polymer, as discussed in Chapter 6, will be constituted from lamellae that are variously aligned and organized in the solid to give a range of microstructures. During the slow crystallization process, the highest melting high molecular weight species will form the first crystallites and the lower molecular weight materials crystallize later. Because of this fractionation process, low molecular weight material either fills the gaps between the lamellae or it segregates to the free surface.

The simplest case would be that of a polymer single crystal grown from solution. Crystals grown in such a manner will have a surface that is predominantly composed of single chains aligned parallel to the surface. The topmost layer of atoms would reflect the surface and since the energy is mostly dominated by short-range interactions the layer will dictate the nature of the surface. If the topmost layer is made up of hydrogen atoms then the surface will have a hydrophobic character. Alternatively, the introduction of oxygen, chlorine, bromine, hydroxyl, carbonyl, *etc.*, groups will make the surface more hydrophilic. This simplified view of the surface is a useful first approximation but is rather inadequate in explaining many of the features observed in real polymer surfaces.

The low molecular weight material segregated at the surface may be more or less disordered than in the ideal single crystal. In the polymer melt there will also exist polymer that has become oxidized, residues of catalysts and processing aids. Often such materials will segregate to an interface. It is therefore not

unusual to find that a measurement of the surface energy, contact angle, *etc.*, indicates a value that is unexpected from consideration of the atomic composition of the bulk polymer. Further evidence for the contaminated nature of the surface can be obtained by washing the surface with a suitable solvent. This process will remove the impurities and low molecular weight material and a new value of the contact angle will be observed. As discussed in Chapter 9, surface roughness can also influence the measured surface energy.

However, in general the surface of a crystalline polymer will have physical properties that correlate well with the chemical structure of the bulk polymer, but may reflect the segregation of end groups to the surface.

10.1.2   Amorphous Polymers

The amorphous state is associated with polymers that are unable to crystallize and form a disordered state. The surface of an amorphous polymer can therefore be pictured as an entangled mass of random coil, pseudo-spherical structures (Figure 10.1).

The polymer surface if the random coils were not to be distorted close to the surface would produce a rough surface that is thermodynamically unstable. Forces in the surface will be imbalanced and as a result either the chains in the surface may move closer together to form a smoother surface, densification, or other regions may expand to fill the voids between the spheres, creating a lower density surface. The latter is not usually the case. As in the case of crystalline polymers, impurities—residual catalysts, processing aids—can segregate to the surface and change the surface energy. The ends of the polymer coil will usually have a slightly different surface energy from the rest of the polymer chain and as a consequence they may segregate to the surface.

As an illustration of the tendency for polymer end groups to segregate to the surface we will consider the case of a polystyrene that has fluorine end caps. The polymer was produced by using a dilithium initiator, and the end cap was
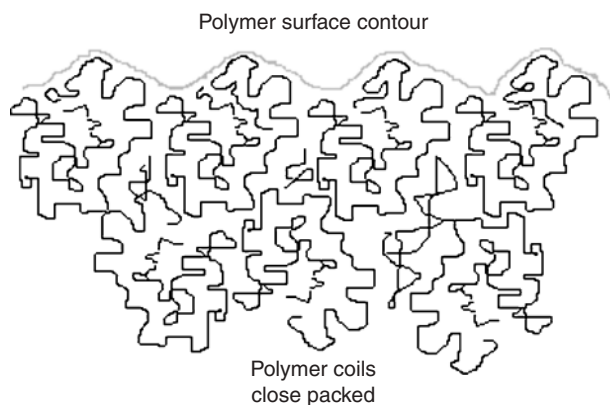
Polymer surface contour

Polymer coils
close packed

Figure 10.1   Schematic of close-packed polymer coils forming a polymer surface.

$(CH_3)_2Si(CH_2)_2(CF_2)_5CF_3$ end function either on one or both ends.[1] The surface was analysed using a combination of X-ray photoelectron spectroscopy (XPS) and secondary ion mass spectrometry (SIMS) that are both very surface sensitive methods. The very surprising result was found that after a few days' annealing of the samples the surface concentration of terminal fluorine substituted groups that was initially about 85% of the atomic composition of the surface increased to almost 100%. The polymers were all of molar mass at or below the entanglement limit and hence there is little constraint for these materials to attempt to achieve their thermodynamically lowest state that would be the surface segregation of the fluorine groups.

10.1.3 Polymer Blends

Polymer blends may be expected to reflect the balance of forces that control their phase structure in the bulk. If two polymers are compatible in the bulk, they may or may not segregate in the surface depending on the balance of forces. Materials that are able to phase separate will segregate in the surface, and generally speaking the lower surface energy material will move towards the free air surface. This effect was illustrated in Chapter 9 in the case of the surface segregation of the ether soft block in the case of block polyurethane copolymers.

10.2 Theoretical Description of the Surface of a Polymer

10.2.1 Surface Tension of Homopolymers

The precise value of the surface tension is the result of a number of interactions; however, the values for high polymers vary from about 20 mN m^{-1} for highly hydrophobic materials such as polydimethylsiloxane (PDMS) and polyfluorocarbons to values of the order of 45 mN m^{-1} for polar materials such as polyesters and polyamides. The surface tension of water has a value of 80 and hence most materials are only mildly hydrophilic.

   As with many other features of molecular interactions, averaged values can be used to describe the behaviour of particular functional groups in a molecule. These group contributions have been estimated for a variety of different functional groups, e.g. oxygen in esters, hydroxyl groups, halogens, nitrogen, sulfur, double and triple bonds, *etc.*,[1,2] and provide a simple method of estimating the expected surface tension for an unknown material. In the estimation of many thermodynamic quantities it is possible to use group contributions to calculate the surface tension. The strength of the interactions can be calculated using the dispersive solubility δ^d which can be calculated from tabulated values of dispersive molar attraction constants F_i according to

$$\delta^d = \sum_i \frac{F_i}{\nu} \tag{10.1}$$

where v is the molar volume of the groups/entities from which the polymer is created.[3] Using this approach the surface tension can be calculated for non-polar polymers using the following empirical relationship:

$$\gamma = 0.2575\delta^2\rho^{-1/3} \tag{10.2}$$

where ν is the density in g ml^{-1} and δ is in cal$^{1/2}$ ml$^{-1/2}$. This very simple formula predicts the surface tension to within 5–10% of the measured values for a large number of polymers. In the case of PDMS the group contribution prediction for the backbone is 20.9 mN m^{-1} compared with a value of 20.4 ± 0.07 mN m^{-1} from experiment. One of the interesting problems that can be explored theoretically and is very difficult experimentally is the possible effect of segregation of chain ends into the surface. For non-polar end groups the following expression has been proposed:

$$\gamma = 0.07147\vartheta^{1/3}(\delta^d)^2 \tag{10.3}$$

As indicated in previous chapters, low molar mass materials can segregate to surfaces and hence the molar mass dependence of the surface tension is an important factor in considering the performance of a polymer material. Wu[4] has proposed that

$$\gamma^{1/4} = \gamma_{\infty}^{1/4} - \frac{k}{M} \tag{10.4}$$

where k is a characteristic constant for that polymer system and Le Grand and Gaines[5] have proposed that

$$\gamma = \gamma_{\infty} - \frac{k}{M^{2/3}} \tag{10.5}$$

Both these relationships are theoretically correct and are extremes of the lattice theory, the indices of the molar mass having the value 2/3 for low molar mass and 1 for high molar mass materials.

10.2.2 Theories of Homopolymer Surface Tension

Following the initial approach of Gibbs, the surface tension can be obtained from the equations of state:[5]

$$\gamma = 0.095P^{*2/3}T^*/\tilde{V}^{2.1} \tag{10.6}$$

where P, T and V are, respectively, the pressure, temperature and volume. The asterisks indicate these are characteristic parameters of the equation of state and the tilde indicates a parameter reduced by the characteristic parameter. An alternative approach starts from the generated van der Waals square gradient approach in which the effect of the density gradient across the polymer–air interface is assumed to be a gradual transition. The width of this density gradient depends on the models and the type of polymer and can have

values between 1 and 100 mm depending on the system. The main change in the density will run over a dimension of less than 1 nm, but the density will only reach its equilibrium value at a distance between 5 and 100 nm. Because the reduced free energy density is dependent on both the reduced temperature and density, it will generally vary through the interface region. The surface tension is related to the excess free energy density $\Delta\tilde{\alpha}$ by

$$\tilde{\gamma} = 2 \int\limits_{-\infty}^{\infty} (\tilde{\kappa}\Delta\tilde{\alpha}|\tilde{\rho}(z)|)^{1/2}\, \partial z \qquad (10.7)$$

where z is the coordinate perpendicular to the surface. Changing the limiting variable produces the equation

$$\tilde{\gamma} = \int\limits_{\tilde{\rho}_{gas}}^{\tilde{\rho}_{liquid}} (\tilde{\kappa}.\Delta\alpha)^{1/2}\, \partial\tilde{\rho} \qquad (10.8)$$

The square gradient coefficient κ is defined by

$$\tilde{\kappa} = -\frac{\partial\tilde{\kappa}_1}{\partial\tilde{\rho}} + \tilde{\kappa}_2 \qquad (10.9)$$

where the first turm on the right-hand side is related to the interaction potential and assumes a value of 0.5 for purely dispersive interactions. The second term arises from non-local entropy effects and is equal to $\tilde{T}/24\tilde{\rho}$. The surface tension is therefore obtained by an integration of the equation of state, $\Delta\tilde{\alpha}(\tilde{\rho}\tilde{T})$. A number of studies have been carried out and by the use of compressible lattice theory it is found to be possible to obtain good agreement between theory and experiment.[1] The reduced surface tension for many different polymers forms a master curve when plotted against reduced temperature which has the following form:

$$\tilde{\gamma} = 0.6109 - 0.06725\tilde{T} - 0.1886\tilde{T}^2 \qquad (10.10)$$

Over small temperature ranges the surface tension varies almost linearly with temperature consistent with the typical linear dependence of density on temperature. The temperature coefficient of surface tension for polymers falls in the range 0.05–0.07 mN m^{-1}.

10.3 Surface Segregation

Most commercial polymer systems are a complex mixture of one or more polymers, plasticizers, antioxidants and processing aids. The surface of such a system will therefore not necessarily be determined by the dominant polymer but will often be influenced by the segregation of low molar mass and low

surface tension materials to the air–polymer interface. Surface segregation can occur with or without the formation of a separate phase at the surface. The segregation of low molar mass materials to the surface can produce changes in refractive index and is sometimes referred to as *blooming*. In this case the component *i* of a miscible mixture adsorbs preferentially to the surface, it produces a change in the surface energy equivalent to $\gamma_i \partial A_i$ where ∂A_i is the surface area occupied by type *i* molecules and γ_i is their surface tension. Following the usual thermodynamic arguments of Gibbs one obtains

$$\sum_{i=1}^{m} n_i \partial \mu_i = \sum_{i=1}^{m} \gamma_i \partial A_i \tag{10.11}$$

It also follows that the surface excess obtained using the classical Gibbs adsorption isotherm is given by

$$-\partial \gamma = \sum_i \Gamma_i \partial \mu_i \tag{10.12}$$

where $\Gamma_i = n_i/A$, in which n_i is the mole fraction of species *i* in the bulk phase. In practical terms lowering the surface energy decreases the thermodynamic work of adhesion and also in practical terms lowers the energy of adhesion of a material stuck to the polymer surface.

10.4 Binary Polymer Blends

In Chapter 8 the principles of phase segregation in polymer blends were considered. As would be expected surface segregation occurs and usually the lower surface energy component of the mixture will tend to appear at the surface. The surface energy can be directly related to the free energy. The techniques for the study of surfaces are discussed in Chapter 9.

The surface composition and near-surface gradient structure of miscible binary homopolymer blends are determined by a balance between the surface energy driving segregation and the exchange free energy that is associated with the near-surface demixing. At equilibrium, this balance represents a minimum in the overall free energy. If the interactions are sufficiently short range in nature, the surface free energy for a planar interface with a sharp density gradient is given by

$$\gamma = \gamma_s(\phi_b) + \int [\gamma_s' + 2(\kappa \Delta F)^{1/2}] \, \partial \phi \tag{10.13}$$

where ϕ_s and ϕ_b refer, respectively, to the surface and bulk volume fractions and γ_s and F are the contributions to the free energy of a unit area of surface and a unit volume of the uniform bulk mixture, respectively. The term $\Delta F = F(\phi) - F(\phi_b^-) - (\phi - \phi_b^-)(\partial F/\partial \phi)_b$ is the free energy cost to exchange composition in the near-surface gradient which eventually balances with the

free energy decrease, $\gamma'_s = \partial\gamma_s/\partial\phi$, associated with the lowering of surface energy upon adsorption of the low surface energy polymer at the surface. In the weak segregation limit, the square gradient coefficient κ which is related to the nature of the inter atomic potential takes the form

$$\kappa = \frac{a^2}{36\phi(1 - \phi)} \qquad (10.14)$$

the polymers being assumed to be symmetric and with identical statistical segment lengths a. The exchange free energy ΔF can be calculated from the Flory–Huggins form for the free energy of mixing:[7]

$$F(\phi_A) = \left[\frac{\phi_A}{N_A}\right]\ln\phi_A + \left[\frac{(1 - \phi_A)}{N_A}\right]\ln(1 - \phi_A) + \phi_A(1 - \phi_A)\chi \qquad (10.15)$$

where N_A and N_B are the number of lattice units per chain for the two blend components A and B, respectively.[1] The surface composition is obtained by minimizing the surface tension in eqn (10.13) with respect to the surface composition and yields a boundary condition:

$$-\gamma_s = \pm 2(\kappa\Delta F)^{1/2}\Big|_{\phi=\phi_0} \qquad (10.16)$$

The surface composition gradient can be calculated from the theory, since

$$\frac{\partial\phi}{\partial z} = \pm 2(\kappa\Delta F)^{1/2} \qquad (10.17)$$

which leads to

$$\phi(z) = -\int_{\phi_b}^{\phi_s} \left(\frac{z}{\Delta F}\right)^{1/2} \partial\phi \qquad (10.18)$$

Using experimentally determined binary interaction parameters, the statistical segment length and the surface energy difference between the blend components, the surface composition and the surface concentration profile can be calculated. The profiles obtained closely approximate to an exponential decay:

$$\phi(z) \cong \phi_b + (\phi_s - \phi_b)\exp\left(-\frac{z}{\xi}\right) \qquad (10.19)$$

Equation (10.19) indicates that the surface decay length ξ conveniently characterizes the concentration profile. For a strongly segregated system the decay length is small but becomes large, ~ 10–20 nm, when the concentration fluctuations grow near the critical point. Experimental studies demonstrate that the surface composition scales directly with the surface energy difference between the constituents.[8]

10.5 End Functionalized Polymers

The end functions of many polymers arise as a consequence of the way the reaction has been either initiated or terminated. The end group of a homo-polymer will also have a different energy from that of the bulk of the main chain, as discussed in Chapter 7. As a consequence the surface interaction parameter has the form

$$\chi_s = \frac{(\gamma_e - \gamma_r)}{kT} \tag{10.20}$$

where the subscripts e and r refer to the two components: the end and repeat units, respectively. As a consequence the concentration profiles are as follows:

- The zone next to the surface has an excess of end groups when χ_s is negative.
- The zone next to the surface is depleted of end groups when χ_s is positive.
- The segregation layer is typically about 1 nm.

Studies of fluorosilane-terminated polystyrene (PS-F)[9–11] illustrate this effect (Table 10.1). The data in Table 10.1 indicate that as the molar mass of the end capped PS-F varies so the extent to which end group segregation varies. The highest molar mass polymer has a value approaching that of normal polystyrene. Studies of blends of PS with PS-F indicate that the PS-F is preferentially segregated at the surface. It is quite surprising that such a small component of the bulk can have such an effect on the surface and illustrates the importance of the differential surface energy in controlling the composition of the surface layer.

10.6 Phase Segregation and Enrichment at Surfaces

Perdeuterated poly(methyl methacrylate) is thermodynamically slightly differ-ent from poly(methyl methacrylate) This difference in surface energy which is

Table 10.1 Various data for fluorosilane-terminated polystyrene (PS-F).

Polymer	M_n by GPC[a]	Functionality	Surface tension (mN m^{-1})	Surface fraction of end groups
Polytetrafluoroethylene			18.2	
5K PS-F	5,300	0.89	19.9	0.87
11K PS-F	10,900	0.78	22.1	0.72
25K PS-F	25,000	0.85	24.1	0.58
148K PS-F	148,000	1.00	29.7	0.19
Polystyrene			32.4	

[a] GPC, gel permeation chromatography.

estimated to be 0.08 mJ m^{-2} is sufficient to allow the perdeuterated polymer to become enriched at the surface. A study of neutron reflectivity and SIMS clearly indicates that surface enrichment is occurring and also demonstrates how the data from these two methods can be combined to allow quantification of the slow diffusion of the species to the surface. Small differences in the thermodynamics of the blend are sufficient to achieve the surface segregation (Figure 10.2).

Atomic force microscopy (AFM) combined with XPS and X-ray reflectivity measurements carried out on deuterated polystyrene and polystyrene containing 1% bromine blends indicate that the surface segregation can be quite marked and depends on the relative composition of the blend (Figure 10.2). The different topographical features arise from the effects of spinodal decomposition of the polymer mixtures during film formation. The initial structures (Figure 10.2a) resemble haystacks and are small islands of the brominated polystyrene. Identification of the nature of the islands is possible through the comparison of the changes in the SIMS spectra as the composition of the mixture is changed. The small haystacks are quite regular and correspond to dimensions that are a little greater than the random coil radius for the polymers. The height of the features is of corresponding dimensions. Increasing the composition leads to a growth in the size of these features as shown in Figure 10.2b. A co-continuous phase structure is observed at a composition of 60% and at higher compositions of the poly(brominated styrene) the surface takes on a cheese-like structure. The depth of the holes has dimensions that are
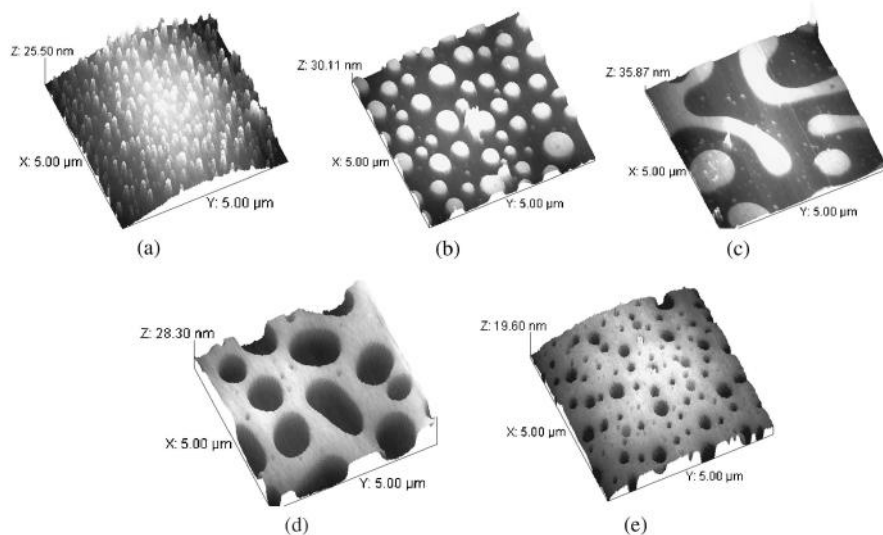

Figure 10.2 AFM images of the surface of polystyrene-d$_8$/poly(1.0% brominated styrene) [P(Br$_{1.0}$S)] blends:[14] (a) 10%, (b) 50%, (c) 60%, (e) 70% and (d) 90%.

once more close to the mean square radius of gyration of the polymer phase indicating that the topography is of the order of the size of a polymer molecule.

10.7 Electrohydrodynamic (EHD) Instabilities in Polymer Films

An interesting feature of the balance of forces which exists at a surface is demonstrated when a thin layer of a polymeric liquid or solution is placed in an electric field.[15–17] The original theory considered the dynamic instability which is created when a dielectric media, polymer liquid, is sandwiched between a conductive liquid and a conductive substrate (Figure 10.3).

It has been shown, however, that provided the gap between the dielectric and another substrate is small, essentially the same EHD instabilities are observed. The equation of motion for the lateral flow of a liquid in a thin film assuming that the fluid is incompressible has the form

$$\frac{\partial}{\partial t} h(x, t) = -\frac{\partial}{\partial x} j(x, t) = C \frac{\partial^2}{dx^2} p[h(x, t)] \tag{10.21}$$

where x is the lateral coordinate, $h(x, t)$ is the local film thickness and $j(x, t)$ is the lateral liquid flow in the film, integrated along the normal coordinate. The shape of the flow profile and the viscosity of the liquid are absorbed into the positive constant C. The film pressure, $p(x, t)$, can be written as

$$p = \frac{A}{6\pi h^3} + \frac{\varepsilon \varepsilon_0 U^2}{2h^2} - \sigma \frac{\partial^2 h}{\partial x^2} \tag{10.22}$$

The first term is the disjoining pressure in the film with A the Hamaker constant describing the van der Waals interaction of the film with the surrounding media. The second term represents the electrostatic pressure exerted on the film by an electrostatic potential difference, U, between the conducting media cladding the film, with ε being the dielectric constant of the film material. Finally the third term describes the Laplace pressure in the film with σ donating the interface tension between the film and the upper (liquid) medium.

The liquid will be in thermal motion and there will be a small fluctuation in the thickness in an initially homogeneous film of thickness h_0.
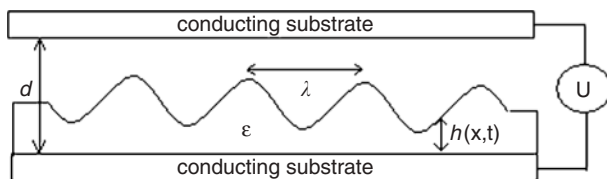

Figure 10.3   Schematic of the EHD experiment.

Equation (10.21) gives

$$-C^{-1}\frac{\partial h}{\partial t} = \left(\frac{A}{2\pi h_0^4} + \frac{\varepsilon\varepsilon_0 U^2}{h_0^3}\right)\frac{\partial^2 h}{\partial x^2} + \sigma\frac{\partial^4 h}{\partial x^4} \qquad (10.23)$$

The overall pressure distribution at the film surface can be written as

$$p = p_0 - \gamma\frac{\partial^2 h}{\partial x^2} + p_{el}(h) + p_{dis}(h) \qquad (10.24)$$

where p_0 is atmospheric pressure, the second term stems for the surface tension γ and the fourth term, the disjoining pressure p_{dis}, arises from dispersive van der Waals interactions. The electrostatic pressure for a given electric field in the polymer

$$E_p = \frac{U}{\varepsilon_p d - (\varepsilon_p - 1)h} \qquad (10.25)$$

is given by

$$p_{el} = -\varepsilon_0\varepsilon_p(\varepsilon_p - 1)E_p^2 \qquad (10.26)$$

For a sufficiently high voltage only the electrostatic interactions need to be considered. In a stability analysis, a small perturbation of the interface with wave number q, the growth rate τ^{-1} and amplitude u is considered: $h(x,t) = h_0 + u\exp[(iqx + t)/\tau]$. The modulation of h gives rise to the lateral pressure gradient inside the film inducing a Poiselle flow j:

$$j = \frac{h^3}{3\eta}\left(-\frac{\partial p}{\partial x}\right) \qquad (10.27)$$

where η is the viscosity of the liquid. A continuity equation enforces mass conservation of the incompressible liquid:

$$\frac{\partial j}{\partial x} + \frac{\partial h}{\partial t} = 0 \qquad (10.28)$$

Combining eqn (10.24), (10.27) and (10.28) a differential equation is obtained that describes the dynamic response of the interface to the perturbation. In a linear approximation a dispersion relation is obtained:

$$\frac{1}{\tau} = \frac{h_0^3}{3\eta}\left(\gamma q^4 + \frac{\partial p_{el}}{\partial h}q^2\right) \qquad (10.29)$$

Fluctuations are amplified if $\tau > 0$. Since $\partial p_{el}/\partial h < 0$, all modes with

$$q < q_c = \sqrt{-\frac{1}{\gamma}\frac{\partial p_{el}}{\partial h}}$$
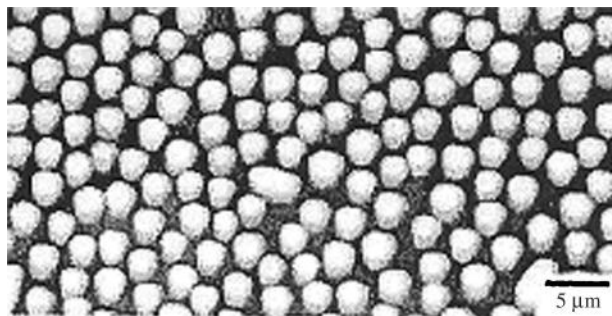
Figure 10.4   AFM image of a 115 nm thick brominated polystyrene film annealed for 1 h at 170 °C. The nearest neighbour distance between the columns is ~ 3 μm.

are unstable. With time, the fastest growing fluctuation will eventually dominate, corresponding to the maximum in eqn (10.29):

$$\lambda = 2\pi \sqrt{\frac{\gamma U}{\varepsilon_0 \varepsilon_p (\varepsilon_p - 1)^2} E_p^{-3/2}} \qquad (10.30)$$

It has been shown that application of an electric field causes the polymer to become localized into specific regions and to take on a vertical columnar structure, leaving the regions around the column depleted of polymer (Figure 10.4). This process is similar that which occurs during spinodal decomposition and is responsible for the structures that are illustrated in Figure 10.2.

An extensive discussion of the data on surface segregation can be found elsewhere.[12–14]

The consideration of the polymer surface allows a number of important technological issues to be specifically addressed: contact angle and surface energy data, high porosity, lack of gloss in transparent films, *etc*.

Recommended Reading

R.A.L. Jones and R.W. Richards, *Polymers at Surfaces and Interfaces*, Cambridge University Press, Cambridge, 1999.
J.T. Koberstein, *Encyclopaedia of Polymer Science and Technology*, John Wiley, 2002.

References

1. S. Affrossman, P. Bertrand, M. Hartshorne, T. Kiff, D. Leonard, R.A. Pethrick and R.W. Richards, *Macromolecules*, 1996, **29**, 5432.

2. J.T. Koberstein, *Encyclopaedia of Polymer Science and Technology*, John Wiley, 2002.
3. D.W. Van Krevelen, *Properties of Polymers*, Elsevier, 1980, p. 163.
4. S. Wu, *Polymer Interface and Adhesion*, Marcel Dekker, New York, 1982.
5. D.G. Le Grand and G.L. Gaines, *J. Colloid Interf. Sci.*, 1969, **31**, 162.
6. G. Patterson and A.K. Rastogi, *J. Phys. Chem.*, 1970, **74**, 1076.
7. P.J. Flory, *Principles of Polymer Chemistry*, Cornell University Press, Ithaca, NY, 1971.
8. Q.S. Bhatia D.H. Pan and J.T. Koberstein, *Macromolecules*, 1988, **21**, 353.
9. S. Affrossman, *Macromolecules*, 1994, **27**, 1588.
10. J.F. Elman, *Macromolecules*, 1994, **27**, 5341.
11. M.O.J. Hunt, *Macromolecules*, 1993, **26**, 4854.
12. R.A.L. Jones and R.W. Richards, *Polymers at Surfaces and Interfaces*, Cambridge University Press, Cambridge, 1999.
13. I. Hopkinson, F.T. Kiff, R.W. Richards, S. Affrossman, M. Hartshorne, R.A. Pethrick, H. Munro and J.R.P. Webster, *Macromolecules*, 1995, **28**, 627.
14. S. Affrossman, G. Henn, S.A. O'Neil, R.A. Pethrick and M. Stamm, *Macromolecules*, 1996, **29**, 5010.
15. E. Schaffer, T. Thurn-Albrecht, T.P. Russel and U. Steiner, *Europhys. Lett.*, 2001, **53**(4), 518.
16. M.D. Dickey, E. Collister, A. Raines, P. Tsiartas, T. Holcombe, S.V. Sreenivasan, R.T. Bonnecaze and C. Grant Wilson, *Chem. Mater.*, 2006, **18**, 2043.
17. S. Herminghaus, *Phys. Rev. Lett.*, 1999, **83**(12), 2359.